

University of Windsor

Scholarship at UWindor

Electronic Theses and Dissertations

Theses, Dissertations, and Major Papers

1-1-1971

Streamwise curvature effects on turbulent wall jet heat transfer.

J. P. Lozon

University of Windsor

Follow this and additional works at: <https://scholar.uwindsor.ca/etd>

Recommended Citation

Lozon, J. P., "Streamwise curvature effects on turbulent wall jet heat transfer." (1971). *Electronic Theses and Dissertations*. 6688.

<https://scholar.uwindsor.ca/etd/6688>

This online database contains the full-text of PhD dissertations and Masters' theses of University of Windsor students from 1954 forward. These documents are made available for personal study and research purposes only, in accordance with the Canadian Copyright Act and the Creative Commons license—CC BY-NC-ND (Attribution, Non-Commercial, No Derivative Works). Under this license, works must always be attributed to the copyright holder (original author), cannot be used for any commercial purposes, and may not be altered. Any other use would require the permission of the copyright holder. Students may inquire about withdrawing their dissertation and/or thesis from this database. For additional inquiries, please contact the repository administrator via email (scholarship@uwindsor.ca) or by telephone at 519-253-3000ext. 3208.

STREAMWISE CURVATURE EFFECTS ON
TURBULENT WALL JET HEAT TRANSFER

A THESIS

Submitted to the Faculty of Graduate Studies
through the Department of Mechanical
Engineering in partial fulfilment of the
requirements for the Degree of Master
of Applied Science at the University of Windsor

by

J. P. Lozon

B.A.Sc., University of Windsor,

Windsor, Ontario, 1968

Windsor, Ontario, Canada

1971.

UMI Number: EC53089

INFORMATION TO USERS

The quality of this reproduction is dependent upon the quality of the copy submitted. Broken or indistinct print, colored or poor quality illustrations and photographs, print bleed-through, substandard margins, and improper alignment can adversely affect reproduction.

In the unlikely event that the author did not send a complete manuscript and there are missing pages, these will be noted. Also, if unauthorized copyright material had to be removed, a note will indicate the deletion.

UMI[®]

UMI Microform EC53089

Copyright 2009 by ProQuest LLC.

All rights reserved. This microform edition is protected against unauthorized copying under Title 17, United States Code.

ProQuest LLC
789 E. Eisenhower Parkway
PO Box 1346
Ann Arbor, MI 48106-1346

ABF 3356

Approved by: J. P. Mathew.
H. J. Tucker.
S. diDion.

345625

ABSTRACT

An experimental study of the heat transfer from a heated circular cylindrical aluminum wall to a bounded air jet blowing over it is presented. The jet was initially at ambient temperature and was considered to be incompressible since the maximum jet velocity was 150 ft./sec. Velocity and temperature profiles were measured at various stations for two temperatures, three Reynolds numbers and three cylinder radii. Heat transfer data were obtained from the Colburn analogy between heat transfer and skin friction (combined with Preston's method of measuring skin friction). Heat flow sensors were also used to measure heat transfer but the results were unsatisfactory and were disregarded.

A correlation was made between the Nusselt number, the Reynolds number and the downstream distance as follows:

$$(\text{Nu})_t = C_1 (\text{Re})_t^{C_2} (x/t)^{-C_3}$$

The numerical values of the empirical constants C_1 , C_2 and C_3 did not change appreciably for the three cylinders investigated.

The Nusselt numbers for the curved wall jets were lower than those for the plane wall jet and exhibited a stronger dependency on downstream distance.

ACKNOWLEDGEMENTS

The author is grateful to Professor W. G. Colborne, Head of the Department of Mechanical Engineering for providing the opportunity and the support for the investigation.

The author wishes to express his gratitude to Dr. K. Sridhar for his supervision, generous aid and encouragement throughout this work.

Thanks are due to Mr. O. Brudy and Mr. R. Myers for their technical assistance in building the test facility. The author is indebted to Miss Jean Inglis for typing the thesis and assisting in corrections.

The research for this thesis was supported by the National Research Council of Canada, Grant Number A-2190.

TABLE OF CONTENTS

	Page
ABSTRACT	iii
NOTATION	viii
LIST OF TABLES	x
LIST OF FIGURES	xi
CHAPTER I	
INTRODUCTION	1
CHAPTER II	
LITERATURE SURVEY	2
2.1 FLOW CHARACTERISTICS OF PLANE WALL JET	2
2.2 FLOW CHARACTERISTICS OF CURVED WALL JET	3
2.3 HEAT TRANSFER IN PLANE WALL JET	4
2.4 HEAT TRANSFER IN CURVED WALL JET	7
2.5 SCOPE OF PRESENT STUDY	8
CHAPTER III	
TEST FACILITIES	9
3.1 AIR SUPPLY	9
3.2 FLOW STRAIGHTENING SECTION	9
3.3 END PLATES AND SUPPORTING TABLE	10
3.4 TEST SURFACE	11
3.5 TRAVERSING MECHANISM	11
3.6 PROBING EQUIPMENT	12
CHAPTER IV	
EXPERIMENTAL PROCEDURE	14

	Page
4.1 CALIBRATION	14
4.2 COLD RUNS	15
4.3 HOT RUNS	15
CHAPTER V	
EXPERIMENTAL RESULTS	17
5.1 REDUCTION OF EXPERIMENTAL DATA	17
5.2 VELOCITY PROFILES	18
5.3 TEMPERATURE PROFILES	18
5.4 HEAT TRANSFER	20
CHAPTER VI	
CONCLUSIONS	24
APPENDICES	
APPENDIX A	26
Analogy Between Heat Transfer and Skin Friction	
APPENDIX B	29
Preston's Method for Calculating Skin Friction	
APPENDIX C	32
Micro-Foil Heat Flow Sensors	
APPENDIX D	35
Integration Method	
APPENDIX E	37
A Note on Error	
LIST OF REFERENCES	40
TABLES	43

	Page
FIGURES	53
VITA AUCTORIS	82

NOTATION

t	width of the nozzle exit (L)
R	radius of the cylinder (L)
θ	angular position along the wall measured from the nozzle exit (degrees)
x	distance measured along the wall from the nozzle exit in the jet flow direction (L)
y	distance measured normal to the surface of the wall (L)
$y_m/2$	larger value of y where $u = 0.5u_m$ (L)
z	distance in the spanwise direction from the jet centreline (L)
d	pitot tube diameter (L)
s	thickness of the flat pitot tube (L)
U_0	average jet velocity at the nozzle exit (ft./sec.)
u	jet velocity component in the x-direction (ft./sec.)
u_m	local maximum value of u (ft./sec.)
c_p	specific heat of air (BTU/slugs/°F)
k	thermal conductivity of air (BTU/hr./ft./°F)
μ	dynamic viscosity of air (lb.sec./ft. ²)
ν	kinematic viscosity of air (ft. ² /sec.)
ρ	density of air (slugs/ft. ³)
h	local heat transfer coefficient (BTU/hr./ft. ² /°F)
q	heat flow rate (BTU/hr./ft. ²)
q_0	local heat flow rate at the wall (BTU/hr./ft. ²)
p	static pressure at a height y (lb./ft. ²)
p_w	static pressure at the wall (lb./ft. ²)
p_a	atmospheric pressure (lb./ft. ²)
P_0	total pressure in the jet (lb./ft. ²)

T	static temperature in the jet ($^{\circ}\text{F}$)
T_p	temperature measured by thermocouple probe ($^{\circ}\text{F}$)
T_a	ambient temperature ($^{\circ}\text{F}$)
T_w	wall temperature ($^{\circ}\text{F}$)
T_f	film temperature = $(T_w + T_a)/2$, ($^{\circ}\text{F}$)
r	temperature recovery factor
\mathcal{Z}_o	wall skin friction (lb_f/ft^2)
c_f	skin friction coefficient ($\mathcal{Z}_o/1/2 \rho u_m^2$)
u_*	local shear velocity = $(\sqrt{\mathcal{Z}_o/\rho})$ (ft./sec.)
$(\text{Nu})_t$	jet exit Nusselt number (ht/k)
$(\text{Nu})_x$	local Nusselt number (hx/k)
Pr	Prandtl number ($c_p \mu g_c/k$)
$(\text{Re})_t$	jet exit Reynolds number ($U_o t/\nu$)
$(\text{Re})_x$	local Reynolds number ($u_m t/\nu$)
$(\text{St})_t$	jet exit Stanton number ($h/\rho c_p U_o$); $(\text{Nu}/\text{RePr})_t$
$(\text{St})_x$	local Stanton number ($h/\rho c_p u_m$); $(\text{Nu}/\text{RePr})_x$
g	gravitational acceleration = 32.2 (ft./sec. 2)
J	mechanical equivalent of heat = 778 (ft.lb./BTU)
C_1, C_2, C_3	empirical constants used in heat transfer correlations
K_1, K_2, K_3	empirical constants used in temperature correlations

SUBSCRIPTS:

a	ambient
m	maximum
o	nozzle exit
w	wall
x	downstream distance

LIST OF TABLES

TABLE		Page
I	Measuring Equipment	43
II	Traverse Locations	44
III	Jet Flow Parameters (0.089 in. nozzle)	45
IV	Jet Flow Parameters (0.132 in. nozzle)	46
V	Jet Flow Parameters (0.250 in. nozzle)	47
VI	Comparison of Temperature Profile correlations	48
VII	Heat Transfer (Nusselt numbers) (Colburn Analogy)	49
VIII	Heat Transfer (Nusselt numbers) (Integration Method)	50
IX	Heat Transfer Correlations (Integration Method)	51
X	Comparison of Heat Transfer Correlations	52

LIST OF FIGURES

FIGURE		Page
1	Curved Wall Jet Nomenclature	53
2	Schematic Diagram of Test Facilities	54
3	Test Facilities	55
4	Test Surface and Traversing Mechanism	56
5	Layout of Test Surface	57
6	Total Pressure Probe	58
7	Temperature Probe	59
8	Velocity Distribution at Nozzle Exit (0.132 in. nozzle)	60
9	Non-Dimensional Velocity Profiles (6.63 in. cyl., 0.132 in. nozzle)	61
10	Non-Dimensional Velocity Profiles (4.00 in. cyl., 0.132 in. nozzle)	62
11	Non-Dimensional Velocity Profiles (3.00 in. cyl., 0.132 in. nozzle)	63
12	Comparison of Velocity Profiles for Heated and Unheated Walls (6.63 in. cyl., 0.089 in. nozzle, $\theta = 60^\circ$)	64
13	Comparison of Velocity Profiles for Heated and Unheated Walls (3.00 in. cyl., 0.089 in. nozzle, $\theta = 60^\circ$)	65
14	Effect of Varying Reynolds Number on Velocity Profiles (6.63 in. cyl., $\theta = 45^\circ$)	66
15	Non-Dimensional Temperature Profiles (6.63 in. cyl., 0.250 in. nozzle, 30°F Hot Run)	67
16	Non-Dimensional Temperature Profiles (6.63 in. cyl., 0.250 in. nozzle, 60°F Hot Run)	68

FIGURE		Page
17	Non-Dimensional Temperature Profiles (4.00 in. cyl., 0.250 in. nozzle, 30°F Hot Run)	69
18	Non-Dimensional Temperature Profiles (4.00 in. cyl., 0.250 in. nozzle, 60°F Hot Run)	70
19	Non-Dimensional Temperature Profiles (3.00 in. cyl., 0.250 in. nozzle, 30°F Hot Run)	71
20	Non-Dimensional Temperature Profiles (3.00 in. cyl., 0.250 in. nozzle, 60°F Hot Run)	72
21	Effect of Varying Reynolds Number on Temperature Profiles (6.63 in. cyl., 60°F Hot Run, $\theta = 45^\circ$)	73
22	Effect of Streamwise Curvature on Temperature Profiles (0.250 in. nozzle, 60°F Hot Run, $\theta = 45^\circ$)	74
23	Logarithmic Temperature Profiles (6.63 in. cyl., 0.089 in. nozzle, 60°F Hot Run)	75
24	Logarithmic Temperature Profiles (4.00 in. cyl., 0.089 in. nozzle, 60°F Hot Run)	76
25	Logarithmic Temperature Profiles (3.00 in. cyl., 0.089 in. nozzle, 60°F Hot Run)	77
26	Heat Transfer Correlations (6.63 in. cylinder and Plane Wall Jet)	78
27	Heat Transfer Correlations (4.00 in. cylinder and Plane Wall Jet)	79
28	Heat Transfer Correlation (3.00 in. cylinder)	80
29	Comparison of Heat Transfer Correlations	81

CHAPTER I

INTRODUCTION

A "wall jet", as first described by Glauert (Ref.1), refers to the flow of a jet along a plane surface. It has been further shown by other investigators that a plane bounded jet will attach to a nearby solid surface and flow along it. This phenomenon is called the Coanda effect and such a flow over a curved wall is called a curved wall jet.

The next advancement made in the study of wall jets was to heat the plane wall or the jet itself and study the heat transfer characteristics of the flow. The results show that this flow arrangement is very useful in obtaining high heat transfer over large surface areas with many applications in such areas as heat exchangers, drying operations and heating operations which involve heat transfer between a gaseous flow and a solid surface.

Since most practical applications for heated wall jets involve a curved surface, information about this type of flow would be very useful. The present investigation aims to provide information on jet flow over a heated curved wall. The variables in this experimental study are Reynolds number, surface temperature and wall curvature.

CHAPTER II

LITERATURE SURVEY

The present study is concerned with wall jet heat transfer and therefore this chapter will deal mainly with the heat transfer characteristics of this problem. A thorough knowledge of the flow characteristics of wall jets is also important but since there are many excellent references available on this subject, only a brief summary will be given here for this area of study.

2.1 FLOW CHARACTERISTICS OF PLANE WALL JET

A theoretical analysis of both laminar and turbulent plane wall jets was first given by Glauert (Ref.1). He showed that similarity existed for laminar flows but complete similarity was not possible over the entire wall jet for the turbulent flows. He also made a study of radial wall jets and predicted their characteristics. Bakke (Ref.2) experimentally investigated the radial wall jet and showed that Glauert's predictions were correct. Sigalla (Ref.3) performed experiments to determine the skin friction distribution along the wall in a plane turbulent jet using Preston's method (Ref.4). Schwarz and Cosart (Ref.5) measured velocity profiles and solved the integral momentum equation to obtain skin friction coefficients. Their skin friction values were twice those presented by Sigalla. Myers, Schauer and Eustis (Ref.6) analytically predicted jet thickness, maximum velocity decay and shear

stress by using the momentum integral method. They also experimentally studied the plane wall jet measuring the shear stress using a 'hot film technique' and compared their results with those calculated from measured velocity profiles. Seban and Back (Ref.7) experimentally measured the skin friction from the velocity profiles for very small values of free stream velocity.

2.2 FLOW CHARACTERISTICS OF CURVED WALL JET

Newman (Ref.8) studied incompressible turbulent wall jet flow over a cylinder (Fig.1) using dimensional and theoretical analysis and confirmed his results by experimental measurement. His theoretical analysis was based on the assumptions that the velocity profiles were similar, the streamlines were circles about the cylinder centre, the skin friction was negligible and flow momentum was almost conserved. Nakaguchi (Ref.9) theoretically analyzed and performed experimental studies on jet flow along a curved wall. He observed that the velocity profiles were very similar to those of a free turbulent jet except in the small portion of the flow close to the wall. He found that turbulent mixing and centrifugal forces influenced the characteristics of the jet. Fekete (Ref.10) made certain improvements on Newman's equipment (Ref.8) and carried out an experimental study. His experimental velocity profiles agreed with Glauert's theoretical predictions for plane wall jets over a large portion of the flow. The results

showed that large differences occurred in the regions approaching separation. Giles, Hays and Sawyer (Ref.11) studied turbulent jet flow on logarithmic spiral surfaces. They found that similarity of the velocity profiles existed everywhere along the jet and that the rate of jet growth was much higher than for jets along circular cylinders at corresponding downstream distances. Sridhar and Tu (Ref.12) in their study of curvature effects on turbulent wall jets concluded that the inner layer velocity profile was affected by streamwise curvature while the mean non-dimensional velocity profiles were not appreciably affected.

2.3 HEAT TRANSFER IN PLANE WALL JET

Zerbe and Selna (Ref.13) obtained an empirical equation for the heat transfer to a flat wall from a plane heated air jet flowing tangentially along the surface.

The correlation for the experimental data was given as:

$$(\text{Nu})_x = 0.071 (\text{Re})_x^{0.8} (x/t)^{-0.6} \quad \dots(2.1)$$

valid for the ranges $(6000 < (\text{Re})_x < 44000)$
 $(15 < x/t < 196)$

Jakob, Rose and Spielman (Ref.14) studied experimentally heat transfer from a heated two-dimensional turbulent air jet to a flat asbestos ebony plate with water vapor entrainment from the surrounding air. The jet nozzle was offset from the wall. The local heat transfer coefficients were calculated using the difference between the maximum local jet temperature and the local

wall surface temperature. The results were correlated as:

$$(\text{Nu})_x = 0.105 (\text{Re})_x^{0.8} (x/t)^{-0.4} \quad \dots(2.2)$$

valid for the ranges $(1340 < (\text{Re})_x < 2.94 \times 10^6)$
 $(15 < x/t < 126)$

Seban and Back (Ref.7) found that the temperature profiles for an adiabatic wall which they measured experimentally were in close agreement with the theoretically predicted profiles if a slight alteration of the theoretical eddy diffusivity distribution was made. In the experimental arrangement used there was a small free stream velocity and initially the injection air was heated above the free stream temperature. The heat transfer correlation based on the Colburn analogy (Ref.15) was given as:

$$(\text{St})_t = 0.41 (\text{Re})_t^{-0.3} (x/t)^{-0.60} \quad \dots(2.3)$$

valid for the ranges $(1400 < (\text{Re})_t < 72000)$
 $(30 < x/t < 288)$

Myers, Schauer and Eustis (Ref.16) made an analytical and experimental study of the heat transfer characteristics of a turbulent wall jet. They analytically predicted the local Stanton number and experimentally verified this by using a step-wall temperature distribution. The local thermal boundary layer thickness evaluated by integration was used to non-dimensionalize the distances normal to the wall for plotting the temperature profiles. The results indicated that the temperature profiles were not influenced by Reynolds number and became "fuller" as downstream distance increased. An analytical prediction was made for the effect

of an unheated starting length on the heat transfer and the comparison with the experimental data showed that differences occurred in the exponential values in the equation. This discrepancy was said to be due to the difference between the actual and assumed theoretical temperature profiles. The experimental correlation for the heat transfer was given as:

$$(St)_t = 0.118(Re)_x^{-0.2}(x/t)^{-0.5625} \left[1 - (L/x)^{0.45} \right]^{-0.0625} \dots(2.4)$$

valid for the ranges $(16600 < (Re)_x < 38000)$
 $(40 < x/t < 181)$

where "L" was the unheated starting length.

Akfirat (Ref.17) experimentally measured the local heat transfer coefficients between an isothermal flat plate and a two-dimensional wall jet. His study contained a comparison of his results with previous investigators. He included in his investigation, heat transfer information for both the laminar and transitional regions. The correlation for a fully developed turbulent flow was given as:

$$(Nu)_t = 0.097 (Re)_t^{0.8} (x/t)^{-0.6} \dots(2.5)$$

valid for the ranges $(1385 < (Re)_t < 16620)$
 $(30 < x/t < 80)$

Hu (Ref.18) experimentally determined the heat transfer from a heated plane wall to a two-dimensional wall jet initially at ambient temperature. He observed that the non-dimensional temperature profiles were independent of Reynolds number. The heat transfer coefficients calculated from heat flow measurements agreed quite well with the

Colburn analogy (Ref.15). The correlation obtained in this experimental study was given as:

$$(Nu)_t = 0.079 (Re)_t^{0.8} (x/t)^{-0.54} \quad \dots(2.6)$$

valid for the ranges $(4500 < (Re)_t < 18000)$
 $(24 < x/t < 576)$

2.4 HEAT TRANSFER IN CURVED WALL JET

Schuh and Persson (Ref.19) studied heat transfer in a two-dimensional free jet flow of limited height over a circular cylinder placed symmetrically in the flow. Their results showed that the mean heat transfer coefficients for thin jets which adhered to the surface were 20 percent higher than for the values for unlimited parallel flow case. They attributed this difference to the 'Coanda effect' and to the high turbulence intensity.

Rao (Ref.20) experimentally investigated the heat transfer from a heated semicircular cylindrical wall to a two-dimensional turbulent air jet initially at ambient temperature. He found that the velocity profiles were unaffected by the heating and were quite similar to the unheated curved wall case. He further observed that the non-dimensional temperature profile was not significantly influenced by Reynolds number and the profile became "fuller" as downstream distance increased. The temperature profiles followed a different power law in the region close to the wall ($y/y_{m/2} < 0.1$) and the rest of the jet and were approximately similar in the outer layer for certain downstream regions. The experimental heat

transfer correlation was given as:

$$(\text{Nu})_t = 0.71 (\text{Re})_t^{0.8} (x/t)^{-0.61} \quad \dots(2.7)$$

valid for the ranges $(4500 < (\text{Re})_t < 18000)$
 $(30 < x/t < 400)$

It is seen from a comparison of equations (2.6) and (2.7) that the heat transfer for a curved wall jet is higher than for the plane wall jet.

2.5 SCOPE OF PRESENT STUDY

The literature survey indicated that no work has been done on streamwise curvature effects on wall jet heat transfer. The present investigation was undertaken to provide information on bounded jet flow over heated curved walls and to compare this with the plane heated wall. It may be expected that due to higher turbulent mixing in the curved wall jet, the heat transfer would be higher for the curved wall than for the plane wall. The original aim was to determine the empirical constants C_1 , C_2 and C_3 in the heat transfer correlation and to study their variation with streamwise curvature. In addition, information on the applicability of the Colburn analogy (combined with Preston's method) to the curved wall jet was to be studied by measuring heat transfer independently with heat flow sensors. Three cylinder sizes (6.63 in., 4.00 in. and 3.00 in.) were used in the experimental investigation of streamwise curvature effect on heat transfer.

CHAPTER III

TEST FACILITIES

A schematic diagram is given in Fig. 2 showing the letter code used in the following description of the test facilities. An overall view of the equipment used is shown in Fig. 3. A view of the test surface and traversing mechanism is shown in Fig. 4.

3.1 AIR SUPPLY

Air was supplied by a type E, size 7 Canadian Buffalo blower (B) with a rating of 2000 CFM, 56.1 in. of water S.P., 3500 RPM and 31.9 BHP. The blower was driven by a 40 HP, 550 volts, 3500 RPM General Electric induction motor. The air flow was controlled by a 10 in. blast gate (A) fitted to the blower intake.

A bleeding section (C) with a constant opening was placed at the exit of the blower to reduce air flow through the system while maintaining a large intake flow to prevent excess heat generation by the blower and overheating of the motor. A diffuser section (D) was placed at the inlet of the plenum chamber (G).

3.2 FLOW STRAIGHTENING SECTION

A filter section (F) was placed at the exit of the plenum chamber. It consisted of three layers of 1 in. thick oil impregnated fibreglass filter material held in position by $\frac{1}{2}$ in. mesh galvanized wire. A honeycomb section (H) consisting of 4 in. x $\frac{1}{2}$ in. cell size 10% resin Kraft Resinated Paper was placed after the filter section for the

purpose of removing large eddies in the air flow. Two layers of 30 x 30 mesh, 0.012 in. stainless steel wire cloth were fixed to a wooden frame and placed at the entrance of the contraction section (M) to further remove small eddies in the flow. The contraction section was made in two parts. The first part reduced the opening from 46 in. x 46 in. to 12 in. x 12 in. The second part reduced the exit to 9 in. x 2 in. The wall profile was designed to give zero slope at the inlet and outlet and zero curvature at the outlet. A plexiglas duct (P), 6 in. in length, was placed between the contraction section exit and the nozzle (N). Three converging brass nozzles (N) were used with the exit dimensions: 9 in. x 0.250 in., 9 in. x 0.132 in. and 9 in. x 0.089 in. The nozzles were bolted in turn to the end of the plexiglas duct so that various Reynolds numbers could be obtained. The design criteria used in the flow straightening section were taken from those presented by Sridhar and Turchyn (Ref.25).

3.3 END PLATES AND SUPPORTING TABLE

Two $\frac{3}{8}$ in. thick, 24 in. radius circular plexiglas plates were used as the end-plates (E). One plate was placed on a horizontal supporting table (T) which was provided with leveling screws to achieve correct alignment. The second plate was supported 9 in. above the bottom plate by 1 in. diameter and 9 in. long acrylic rods.

3.4 TEST SURFACE

The layout of the test surface is given in Fig. 5. The test surfaces were aluminum circular cylinders with outside diameters of 6.63 in., 4.00 in. and 3.00 in. with a wall thickness of 0.063 in. The test surface height was 9 in., the same as the jet nozzle span. The surface was heated by a resistance wire heating element wound on a 3 in. diameter transite cylinder placed concentrically inside the test cylinder. The cylinder was closed at both ends by transite end plates of the same diameter as the cylinder. Copper-constantan thermocouples made of 30 gauge wire were embedded in the cylinder surface at 15° intervals from the nozzle exit and at a height of 2 in. above and below the cylinder centreline. The cylinder was held in position by a vertical $3/4$ in. steel rod. Micro-foil heat flow sensors (described in Appendix C) were bonded to the test surface at $\theta = 30^\circ$, 45° and 60° , adjacent to the embedded thermocouples at these positions.

3.5 TRAVERSING MECHANISM

The traversing mechanism is shown in Fig. 4. The mechanism contained a 12 in. dial type micrometer for radial movement and a 12 in. threaded rod for spanwise movement. This arrangement enabled a three-dimensional traverse of the wall jet to be made: the full length in the direction of the flow, 7 in. in the direction normal to the test surface (with an accuracy of 0.001 in.) and 6 in. in the spanwise direction (with an accuracy of 0.01

in.). The radial traverse could be locked to the top end plate at any position to make a traverse of the jet in the normal and spanwise directions. Two probes were mounted on the traversing mechanism, one above the other and 1 in. apart.

3.6 PROBING EQUIPMENT

The probes are shown in Figs. 4, 6 and 7. The total pressure probe was made with flattened stainless steel hypodermic tubing with an opening of 0.002 in. x 0.066 in. The probe was placed at a distance of 0.5 in. above the cylinder centreline. A Lambrecht sloping manometer (with an accuracy of 0.001 in. of water) was used in making the pressure measurements, with atmospheric pressure as the reference pressure.

The temperature probe was a bare copper-constantan thermocouple with a stem diameter of 0.0625 in. The temperature range for which the probe could be used was 0 - 400°F with the flow velocity ranging from 100 ft./sec. to 600 ft./sec. The probe reading was used in conjunction with a correction for dynamic temperature to give a value of static temperature (with an accuracy of 0.5°F). The wall thermocouple and temperature probe readings were taken with a Honeywell millivolt potentiometer (with an accuracy of 0.25°F). All temperature readings were made with reference to a 32°F junction which was maintained at this temperature by a ZEREF ice point reference chamber (with an accuracy of $\pm 0.02^\circ\text{F}$). The wall thermocouples

and temperature probe were connected to the potentiometer through a twenty-four point contact switch.

Details of all the equipment used are listed in Table I.

CHAPTER IV

EXPERIMENTAL PROCEDURE

The experiments were performed in order to determine the effect of streamwise curvature on heat transfer from a heated curved wall to an air jet blowing over it. Two types of tests were used: the cold run test with the wall unheated and the hot run test with the wall heated above the ambient temperature.

4.1 CALIBRATION

Velocity profiles at the nozzle exit and at various stations around the cylinder were measured with a flattened boundary layer pitot probe. Ambient pressure and temperature were used in the calculation of air density. The static pressure variation in the jet was neglected. The jet exit velocity was kept constant at a nominal value of 150 ft./sec. for all three nozzle sizes. The nozzle exit velocity profile for the 0.132 in. nozzle is shown in Fig. 8. It was concluded that the nozzle exit velocity distribution was uniform.

The wall temperature decreased slightly along the cylinder in the jet direction. The maximum difference between the wall temperature at $\theta = 15^\circ$ and $\theta = 90^\circ$ was 3% of the temperature at $\theta = 15^\circ$. An isothermal wall condition would approximately describe the thermal boundary condition of this investigation. However the actual local wall temperatures were used to calculate such quantities as 'h'.

The temperature recovery factor, r , used in calculating static temperature was 0.9. The static temperatures in the jet were calculated from the probe temperature by using the following relation:

$$T = T_p - ru^2/2gc_pJ \quad \dots(4.1)$$

4.2 COLD RUNS

During the cold runs the test cylinder was at ambient temperature. Velocity distributions were obtained at six different downstream locations for each of the nozzles. The traverse was made by fixing the mechanism at a particular location downstream from the nozzle exit and then moving the probe away from the wall in the radial direction. The velocity was measured at thirty to forty different positions in the radial direction.

4.3 HOT RUNS

The blower was adjusted to give a nozzle exit velocity of 150 ft./sec. The test cylinder was heated to the desired temperature by supplying a current to the electric heating element inside the cylinder. The equipment was then left to run until a steady state condition was reached. The test surface temperature was measured by the copper-constantan thermocouples embedded in the surface at the various downstream locations.

During the hot runs, velocity and temperature profiles were measured at six different downstream stations along the jet axis for each Reynolds number and for the two

nominal temperature differences of 30°F and 60°F between the wall and the ambient. The total pressure probe was used for velocity measurements and the bare thermocouple probe was used to measure temperature in the jet. The profiles were obtained by moving the probes radially away from the wall and taking measurements at thirty to forty points across the width of the jet. The profiles included measurements at three designated points which were used to calculate skin friction using Preston's method and heat transfer using Colburn's analogy. Preston's method for calculating skin friction is given in Appendix B and Colburn's analogy is described in Appendix A.

Hot run tests were performed with the heat flow sensors in position on the cylinder surface. The output from each sensor was measured with a microvolt potentiometer and null detector.

CHAPTER V

EXPERIMENTAL RESULTS

5.1 REDUCTION OF EXPERIMENTAL DATA

The fluid was treated as incompressible since the nozzle exit velocity was kept at 150 ft./sec. The static pressure across the jet was considered to be atmospheric. The density of the air was calculated using the barometric pressure and the room temperature. The other temperature dependent fluid properties such as viscosity, specific heat and thermal conductivity were calculated at the film temperature ($T_f = (T_a + T_w)/2$). The velocity measured by the probe was considered to be the axial velocity at the geometric centre of the pitot tube opening. The readings obtained with the thermocouple probe were converted to static temperature by applying a correction factor for dynamic temperature ($T_{dyn} = u^2/2gc_pJ$). Radiation errors in the temperature measurements were considered negligible since the temperature difference between the wall and the probe was of the order of 50°F and the probe size was small (Ref.23).

The experimental data were reduced with the help of an IBM 1620 computer and the output was plotted using a CALCOMP plotter. The input data for the computer program were: barometric pressure, room temperature, manometer reading, y reading, wall temperature and temperature probe reading. The output data were velocity, static temperature

and various dimensionless groups such as Nusselt number and Reynolds number. The velocity and temperature profiles were plotted directly by the computer.

5.2 VELOCITY PROFILES

The velocity profiles were non-dimensionalized using the local maximum value of velocity (u_m) and $y_m/2$, the larger ordinate where $u = 0.5u_m$. The profiles obtained for the three cylinders at various downstream locations are shown in Figs. 9 to 11. Three Reynolds numbers based on the nozzle slot width were used in the investigation. It is seen from these figures that the profiles are approximately similar. The velocity profiles obtained during the hot runs are superimposed upon the profiles of the cold runs in Figs. 12 and 13. It is seen that the profiles are not significantly changed by heating the wall. The profiles at one particular downstream location for the three different nozzle widths are shown in Fig. 14. This figure shows the effect of varying Reynolds number since the nozzle exit velocity remained constant. It is seen that within the experimental range the Reynolds number has no appreciable effect on the velocity profile.

5.3 TEMPERATURE PROFILES

The static temperature in the jet was non-dimensionalized using the wall temperature and the ambient temperature in the following way: $T_{\text{non}} = (T_w - T)/(T_w - T_a)$. The distance from the wall was non-dimensionalized using the

same length scale, $y_{m/2}$, as that used in the velocity profile calculations. Non-dimensional temperature profiles at various downstream locations are shown in Figs. 15 to 20 for the two nominal temperature differences and the three cylinder sizes. The figures show that the temperature profiles are approximately similar. A comparison between the velocity and temperature profiles indicates that the assumption of similarity is a better approximation for the velocity profiles than for the temperature profiles. The profiles at one particular downstream location for the three nozzle widths are shown in Fig. 21 for the 6.63 in. cylinder and a 60°F temperature difference. It is seen that as the Reynolds number decreases the temperature profiles become "fuller". The non-dimensional temperature profiles at $\Theta = 45^\circ$, for the three cylinders and the 0.250 in. nozzle are plotted in Fig. 22 to show that there are no appreciable curvature effects on the temperature profiles.

The temperature distributions across the jet for the three cylinders and the two temperature differences were correlated in the following form:

$$\frac{T_w - T}{T_w - T_a} = K_1 \left[\frac{y}{y_{m/2}} \right]^{K_2} \left[\frac{x}{\tau} \right]^{K_3} \quad \dots(5.1)$$

The values of K_1 , K_2 and K_3 are tabulated in Table VI.

The non-dimensional temperature profiles are replotted

on a logarithmic scale in Figs. 23 to 25. It is seen that the profiles follow one power law across the entire width of the jet.

5.4 HEAT TRANSFER

The Nusselt number was calculated at six downstream locations using the Colburn analogy (see Appendix A). The skin friction coefficient which was required for the calculations in the Colburn analogy was determined by Preston's method (see Appendix B).

Two nominal temperature differences of 30°F and 60°F were used in the investigation. The results tabulated in Table VII show that there was no significant difference in the Nusselt numbers obtained for the two temperature differences, using the Colburn analogy.

The heat transfer was correlated in the following manner:

$$(\text{Nu})_t = C_1 (\text{Re})_t^{C_2} (x/t)^{-C_3} \quad \dots(5.2)$$

where $(\text{Nu})_t$ was calculated from the Colburn analogy based on the nozzle exit velocity, U_0 , and the slot width, t , and $(\text{Re})_t$ was similarly based on U_0 and t . The empirical values of the constants C_1 , C_2 and C_3 were determined using multiple linear regression. The values of C_2 were 0.71, 0.73 and 0.70 for the 6.63 in., 4.00 in. and 3.00 in. cylinders respectively. Since the value of C_2 for plane wall jet investigation was 0.8, C_2 for the present

study was set at 0.8 in order to make a comparison with the plane wall results. The constants C_1 and C_3 were then evaluated again.

The heat transfer data for the three Reynolds numbers are plotted as $(Nu)_t / (Re)_t^{0.8}$ vs. x/t on a logarithmic scale in Figs. 26 to 28. The correlations for the three cylinders are as follows:

$$(6.63 \text{ in. cyl.}): (Nu)_t / (Re)_t^{0.8} = 0.12 (x/t)^{-1.03} \dots (5.3)$$

$$\text{valid for the ranges } (6500 < (Re)_t < 18500) \\ (6 < x/t < 50)$$

Correlation coefficient = 0.98; standard deviation = 0.004

$$(4.00 \text{ in. cyl.}): (Nu)_t / (Re)_t^{0.8} = 0.12 (x/t)^{-1.06} \dots (5.4)$$

$$\text{valid for the ranges } (6500 < (Re)_t < 18500) \\ (6 < x/t < 40)$$

Correlation coefficient = 0.98; standard deviation = 0.009

$$(3.00 \text{ in. cyl.}): (Nu)_t / (Re)_t^{0.8} = 0.11 (x/t)^{-1.04} \dots (5.5)$$

$$\text{valid for the ranges } (6500 < (Re)_t < 18500) \\ (6 < x/t < 30)$$

Correlation coefficient = 0.97; standard deviation = 0.006

On these same plots, typical results obtained using micro-foil heat flow sensors (see Appendix C) at three downstream locations are included. The points indicate that in most cases the heat flow sensor values are higher than those obtained using the Colburn analogy. However, the Nusselt numbers were found to increase with the downstream distance. For this reason, no attempt was

made to correlate the heat flow sensor data.

A third method of calculating heat transfer was attempted but was found to be impractical. This technique involved integration of the product of the velocity and temperature at each point in the profile. The equation was as follows:

$$\frac{\partial}{\partial x} \int_0^{\infty} u(T - T_a) dy = \frac{q_0}{\rho c_p} \quad \dots(5.6)$$

where q_0 is the local heat flow rate at the wall. The procedure used was to find the area under the curve of $u(T - T_a)$ vs. y using the trapezoidal rule and then plot this area against x to determine the slope of the curve at different downstream locations. A detailed explanation of the integration method and the difficulties associated with this method are given in Appendix D. The Nusselt numbers calculated by this method were much higher than the values obtained from the Colburn analogy or the heat flow sensors. Typical values are given in Table VIII. A correlation of the form given in equation (5.2) was attempted using the values calculated from this method (Table IX) but the results were, in general, not satisfactory. The correlation obtained for the 4.00 in. cylinder was satisfactory. However, the correlations obtained for the other two cylinders indicated that the exponent of the dimensionless downstream distance, x/t , was positive which meant that the heat transfer increased with increasing downstream

distance, which is physically impossible. It is further seen from the values of C_1 and C_3 given in Table IX that there is no consistent variation of these coefficients with streamwise curvature. For these reasons the correlations of Table IX were considered to be unacceptable.

Going back to the Colburn analogy method, it is seen from equations (5.3), (5.4) and (5.5) that within the experimental range of the present investigation there are no appreciable effects of streamwise curvature on the variation of C_3 .

However, a comparison (Fig. 29 and Table X) with the plane wall jet correlations (Ref.17, Ref.18) given by equations (2.5) and (2.6) indicate an appreciable difference in the value of C_3 . For any given x/t and $(Re)_t$, the Nusselt number for the plane wall jet is higher than that of the curved wall jets investigated. A comparison (Fig. 29 and Table X) with the curved wall jet correlation (Ref.20) given by equation (2.7) indicate an appreciable difference in the values of both C_1 and C_3 . The previous curved wall jet results indicate a value of C_1 six times higher than the present investigation but the value of C_3 is approximately equal to the value of the plane wall jet studies (Ref.17, Ref.18).

CHAPTER VI
CONCLUSIONS

The heat transfer data obtained by the Colburn analogy (combined with Preston's method) have been correlated as:

$$(\text{Nu})_t = C_1 (\text{Re})_t^{C_2} (x/t)^{-C_3}$$

Within the range of the experiments, the values of C_1 , C_2 and C_3 did not change significantly. However, the Nusselt numbers for the curved wall jets are lower than those of the plane wall jet and exhibit a stronger dependency on downstream distance. Previous results presented by Rao (Ref.20) indicated that the Nusselt numbers for a curved wall jet were much higher than those of the plane wall jet. No physical reason can be given to explain why the present curved wall jet results should be lower than the plane wall jet results. The Colburn analogy used for calculating heat transfer is based on similarity of velocity and temperature profiles. Although the experimental velocity profiles showed approximate similarity, the experimental temperature profiles, for the 30°F hot runs in particular, do not display this same high degree of similarity. This may indicate that the Colburn analogy is not applicable in the present situation. An improvement in the method of heating the curved wall by using individual heating strips should be made to facilitate an additional and independent method of evaluating local heat transfer.

Further experiments should be carried out with larger cylinders to determine the effect of streamwise curvature on heat transfer in the range between the present investigation and the plane wall jet.

APPENDIX A

Analogy Between Heat Transfer
and Skin Friction

Reynolds analogy between heat and momentum transfer can be expressed as:

$$q = -\tau c_p \frac{dT}{du} \quad \dots(A-1)$$

This relationship is valid for both laminar and turbulent flows (Ref.26).

For the case of forced convection turbulent flow over a flat plate, the rate of heat transfer at a point along the plate a distance x from the leading edge is expressed as:

$$q_x = -\tau_x c_p \frac{dT}{du} \quad \dots(A-2)$$

This equation can be rewritten as:

$$\int_0^U q_x du = - \int_{T_w}^{T_a} \tau_x c_p dT \quad \dots(A-3)$$

After integration we obtain:

$$q_x U = \tau_x c_p (T_w - T_a) \quad \dots(A-4)$$

The skin friction coefficient, c_f , is defined as the ratio of the total friction force to the total kinetic energy. For station X , c_f is given as:

$$c_{f_x} = \frac{\tau_x}{\frac{1}{2} \rho U^2} \quad \dots(A-5)$$

By rewriting the rate of heat transfer as:

$$q_x = h_x (T_w - T_a) \quad \dots(A-6)$$

and substituting equations (A-5) and (A-6) into equation (A-4) we obtain:

$$h_x (T_w - T_a) U = c_{f_x} \frac{1}{2} \rho U^2 c_p (T_w - T_a) \quad \dots(A-7)$$

$$\frac{h_x}{\rho c_p U} = \frac{1}{2} c_{f_x} \quad \dots(A-8)$$

The left hand side of equation (A-8) is known as the local Stanton number, $(St)_x$. Equation (A-8) is valid only for $Pr = 1$. The Stanton number is also defined by:

$$(St)_x = \frac{(Nu)_x}{(Re)_x Pr} = \frac{(Nu)_x}{(Re)_x} \quad \dots(A-9)$$

By substituting equation (A-9) into equation (A-8) we obtain:

$$(Nu)_x = \frac{1}{2} c_f (Re)_x \quad \dots(A-10)$$

Equation (A-10), known as Reynolds analogy between heat and momentum transfer, is valid only if the heat resistance through the laminar sublayer is assumed to be negligible since Reynolds did not consider this region in his analogy.

Colburn (Ref.15, Ref.26) developed a correlation of heat transfer and shear stress for $Pr > 0.6$ by modifying Reynolds analogy for a flat plate as given in equation (A-10). His results are given as:

$$(St)_x Pr^{2/3} = 0.0292 (Re)_x^{-0.2} \quad \dots(A-11)$$

$$(5 \times 10^5 < (Re)_x < 10^7)$$

By substituting $(St)_x$ from equation (A-9):

$$(Nu)_x = 0.0292 (Re)_x^{0.8} Pr^{1/3} \quad \dots(A-12)$$

This equation is based upon the skin friction coefficient:

$$c_f = 0.0584 \text{ Re}^{-0.2} \quad \dots(\text{A-13})$$

Equations (A-11) and (A-13) can be combined to give:

$$\text{St Pr}^{2/3} = \frac{1}{2} c_f \quad \dots(\text{A-14})$$

This equation is known as Colburn's analogy between convective heat transfer and shear stress. Equation (A-14) can be rewritten as:

$$\text{Nu} = \text{Pr}^{1/3} \text{Re} \frac{1}{2} c_f \quad \dots(\text{A-15})$$

In the present investigation the value of c_f , the skin friction coefficient, was defined as follows:

$$c_f = \frac{\tau_o}{\frac{1}{2} \rho U_o^2} \quad \dots(\text{A-16})$$

where τ_o is the average value of skin friction at a particular station as determined by Preston's method described in Appendix B.

The procedure used in the present investigation was to take measurements to calculate τ_o and then determine the Nusselt number for the particular station using equation (A-15).

APPENDIX B

Preston's Method for Calculating Skin Friction

Preston (Ref.4) developed a simple technique to determine local turbulent skin friction on smooth surfaces using a round pitot tube which rests on the surface. His purpose in doing this was to obtain a method which could be easily applied in many different situations and give accurate values of skin friction. Previous investigators had used methods such as pressure drop calculations, towing tank tests, overall drag measurements and direct force measurements on small surface elements. These methods required great precision and care and were unsuitable for general use both in the laboratory and in practical situations such as aircraft and ships.

Preston based his technique on the assumption that a limited region existed near the surface where the relation:

$$\frac{u}{u_*} = f\left(\frac{yu_*}{\nu}\right) \quad \dots(B-1)$$

was valid and also independent of pressure gradients and upstream disturbances. This relation implies that in this region local dynamic similarity exists and τ_o , ρ , ν and a representative length are the only independent variables. A relation between the total pressure measured by the pitot tube and the skin friction is given by:

$$\frac{(P_o - p_w)d^2}{\rho \nu^2} = F\left(\frac{\tau_o d^2}{\rho \nu^2}\right) \quad \dots(B-2)$$

Equation (B-2) includes the displacement of the effective

centre and scale effects on the reading of the pitot tube. If geometrically similar circular pitots are used in the prescribed region then the function F holds for all cases including increasing or decreasing pressure gradient at any station along the wall.

Included in Preston's work was a study of skin friction measurements using a flat pitot tube similar to that used in the present investigation. For this type of pitot tube he obtained the relation:

$$\log_{10} \left(\frac{\tau_o y^2}{\rho v^2} \right) = G \left(\frac{(P_o - p) y^2}{\rho v^2} \right) \quad \dots(B-3)$$

For the range $y/s > 2.5$ and $(P_o - p) y^2 / \rho v^2 > 1.5 \times 10^5$

Preston obtained the following calibration:

$$\log_{10} \left(\frac{\tau_o y^2}{\rho v^2} \right) = -1.372 + \frac{7}{8} \log_{10} \left(\frac{(P_o - p) y^2}{\rho v^2} \right) \quad \dots(B-4)$$

The measurements in the present investigation lie within the range given by Preston and therefore the skin friction was calculated from the equation (B-4). The value of s for the flat pitot tube used is 0.006 in. The values chosen for y are 0.040 in., 0.045 in. and 0.050 in. A value of skin friction, τ_o , is determined for each value of y and an average value for τ_o is then calculated.

A discrepancy could come from the fact that Preston's calibration equation was obtained in a wind tunnel and inside circular pipes. In the present investigation, jet flow over a cylinder is considered and the differences in

the velocity profile characteristics could affect the calibration. One of the initial aims of the investigation was to provide information on this point by independent measurements.

APPENDIX C

Micro-Foil Heat Flow Sensors

One method to measure the heat transfer coefficient, h , used the micro-foil heat flow sensor supplied by the RdF Corporation, Hudson, New Hampshire.

The sensor consists of a thin wafer of low density compression resistant insulation enclosed between two 0.00025 in. butt-bonded foil thermocouples. The foils form a low impedance differential thermocouple system which provides an electromotive force proportional to the temperature difference between the wafer faces and measures the heat flow across the very thin wafer.

According to the manufacturer the heat sensor's rapid response makes it suitable for making direct measurements of transient heat fluxes and its low thermal resistance makes it effective in measuring heat transfer between exposed surfaces and their surroundings.

The application of the sensor should be by bonding to the surface with any of several cements, except those that dry by solvent evaporation. Epoxy cement is best for ease of application but the choice depends upon the temperature of the particular surface. Double sided pressure sensitive tape can be used also where thickness and loss of response time is not critical. In the present investigation, epoxy cement was used to bond the sensor to the test surface.

The manufacturer's specifications indicated that the sensor output was of the order of 0.05 microvolts per BTU/hr./ft². The output varies with the surface temperature. A calibration curve over a range of surface temperatures from -300°F to +400°F was supplied by the manufacturer. The change in calibration factors due to a change in base temperature was approximately 0.1% per °F. The surface temperature could be measured by either the embedded wall thermocouples or the thermocouple incorporated in the heat flow sensor. In this present study, the surface temperature was measured by the thermocouple in the heat flow sensor.

In the present investigation, the output from the sensor was found to fluctuate considerably which made it very difficult to obtain an accurate reading of heat flow. The values of the heat transfer coefficient, h , found using the sensors indicated that h increased with increasing downstream distance which is physically impossible in the particular type of flow arrangement used in this experiment. The values of h for most cases were higher than those obtained using the Colburn analogy (combined with Preston's method) but the heat flow sensor values were not used because of the trend showing the increasing values of h . No explanation could be found for this apparent disagreement with the physical nature of the flow. Errors in the heat flow sensor readings

could be caused by the type of cement used for bonding to the surface, by the curvature of the test wall and by the presence of the sensor in a region of high forced convection heat transfer.

APPENDIX D

Integration Method

The integration method of calculating heat transfer involves finding the enthalpy flow rate crossing an area normal to the curved surface. The enthalpy flow rate at a particular point may be expressed as the product of the mass flow rate, $\rho u dy$, the temperature referred to ambient conditions, $(T - T_a)$, and the specific heat, c_p , which can be written as:

$$dH = \rho c_p u (T - T_a) dy \quad \dots(D-1)$$

The total enthalpy flow rate at this station can then be found by integrating equation (D-1).

$$H = \rho c_p \int_0^{\infty} u (T - T_a) dy \quad \dots(D-2)$$

The units of H are BTU/hr./ft. If H is determined at various probing stations, then the surface heat transfer rate at a particular station is found as follows:

$$q_o = \rho c_p \frac{\partial}{\partial x} \int_0^{\infty} u (T - T_a) dy \quad \dots(D-3)$$

This equation is the mathematical statement of the integration method of calculating heat transfer.

Since the velocity, u , and the temperature, T , could only be measured at finite values of y , an approximation must be used to evaluate the integral. This was accomplished by taking measurements of u , T and y and then plotting the product $u(T - T_a)$ vs. y . The area under this curve was found by using the trapezoidal rule.

The derivative, $\partial/\partial x$, also had to be approximated.

The integral was evaluated at various stations at particular distances, x , downstream of the nozzle exit. The value of the integral was then plotted vs. x . The slope of this curve at a particular x was found manually. This slope was used as the approximation of the derivative, $\partial/\partial x$. The heat flow rate, q_0 , at a particular station was calculated by multiplying this value of slope by ρc_p . This q_0 was then used to evaluate the local Nusselt number, $(Nu)_x$, for this station.

The Nusselt numbers calculated by this method were much higher than those found by the Colburn analogy method and the heat flow sensor measurements.

One of the basic difficulties of the integration method was that most of the temperature change occurred in a small region very very close to the wall which could not be probed. This meant that the measurements that were taken to evaluate the integral did not include this very important region. A further difficulty was that the determination of the slope of the curve $\int_0^{\infty} u (T - T_a) dy$ vs. x was very inaccurate and introduced a significant error in the evaluation of q_0 .

These errors make the integration method rather unsuitable as a means of determining the heat flow rate.

APPENDIX E

A Note on Error

In this section a very brief discussion of the errors present in this investigation is given. A complete description of all such errors is not attempted.

For the velocity measurements, errors were present in the manometer readings and the probe positioning. The manometer was accurate to within ± 0.5 mm. giving a possible velocity error of $\pm 5\%$ based on U_0 .

Excluding the dynamic effects, the temperature probe was accurate to within $\pm 0.5^\circ\text{F}$. The maximum dynamic temperature was of the order of 1°F . These could result in a possible temperature error of $\pm 5\%$ based on a 30°F temperature difference.

The accuracy of the traverse was 0.001 in. but the error in positioning the probe could be as large as 0.005 in. since the position of the pitot had to be determined when it was touching the surface.

The Preston method for measuring skin friction is discussed in Appendix B. Errors were present due to the manometer reading and the positioning of the pitot tube at the required distances from the test surface. An estimate of the possible skin friction measurement error is $\pm 4\%$ based on the experimental values determined for τ_0 . A further discrepancy could come from the fact that Preston's calibration was done in a wind tunnel and inside

circular pipes. The present investigation was concerned with an air jet flowing over a convex surface. No estimate of the effect of this difference was attempted.

In this investigation it was assumed that the Colburn analogy was applicable for jet flows over curved surfaces. No attempt was made to check the validity of this assumption. The errors of skin friction measurement also affected the heat transfer values. The errors in the calculation of the Prandtl number and Reynolds number were assumed to be negligible.

The integration method for determining heat transfer as discussed in Section (5.4) and Appendix D was based on the assumption of similarity of velocity profiles and temperature profiles. Although approximate similarity was present, complete similarity was not fully obtained. The determination of the area under the curve by the trapezoidal rule introduced a small error. A very significant error was present in the determination of the slope of the curve at a required point. This error in slope measurement coupled with the lack of similarity of profiles made this method of heat transfer very inaccurate.

The heat flow sensors used for measuring heat transfer were 0.003 in. thick and 0.5 in. square. The sensors were cemented to the surface at the required position. Errors were present due to the disturbances caused by the presence of the sensors in the air flow. Since the sensors were

bonded to the surface, the thickness of the cement under the sensors changed the conductivity between the surface and the sensor. It was found that the sensor output which was of the order of 10-20 μ volts fluctuated considerably. This was assumed to occur because of the high sensitivity of the sensor and the turbulent air flow passing over the sensor. No estimate of error is attempted for the heat flow sensor measurements.

LIST OF REFERENCES

1. Glauert, M. B. "The Wall Jet", Journal of Fluid Mechanics, volume 1, page 625 (1956).
2. Bakke, P. "An Experimental Investigation of a Wall Jet", Journal of Fluid Mechanics, volume 2, page 467 (1957).
3. Sigalla, A. "Measurement of Skin Friction in a Plane Turbulent Wall Jet", Journal of Royal Aeronautical Society, volume 62, no. 576, page 873 (1958).
4. Preston, J. H. "The Determination of Turbulent Skin Friction by Means of Pitot Tubes", Journal of the Royal Aeronautical Society, volume 58, page 109 (1954).
5. Schwarz, W. H.,
Cosart, W. P. "The Two-Dimensional Turbulent Wall Jet", Journal of Fluid Mechanics, volume 10, page 481 (1961).
6. Myers, G. E.,
Schauer, J. J.,
Eustis, R. H. "The Plane Turbulent Wall Jet Part I. The Development and Friction Factor", Department of Mechanical Engineering, Stanford University, Technical Report No. 1 (1961).
7. Seban, R. A.,
Back, L. H. "Velocity and Temperature Profiles in a Wall Jet", International Journal of Heat and Mass Transfer, volume 3, page 255 (1961).
8. Newman, B. G. "The Deflection of Plane Jets by Adjacent Boundaries-Coanda Effect", Boundary Layer and Flow Control, volume 1. edited by G. V. Lachman, Pergamon Press, page 232 (1961).
9. Nakaguchi, H. "Jet Along a Curved Wall", Department of Aeronautics, University of Tokyo, Research Memorandum No. 4 (1961).
10. Fekete, G. I. "Coanda Flow of a Two-Dimensional Wall Jet on the Outside of a Circular Cylinder", McGill University, Report No. 63-11 (1963).

11. Giles, J. A.,
Hays, A. P.,
Sawyer, R. A. "Turbulent Wall Jets on Logarithmic
Spiral Surfaces", The Aeronautical
Quarterly, volume 17 (1966).
12. Sridhar, K.,
Tu, P. K. C. "Experimental Investigation of
Curvature Effects on Turbulent
Wall Jets", Journal of Royal
Aeronautical Society, volume 73,
page 977 (1969).
13. Zerbe, J.,
Selna, J. "An Empirical Equation for the
Coefficient of Heat Transfer to a
Flat Surface from a Plane Heated Air
Jet Directed Tangentially to the
Surface", NACA TN-1070 (1946).
14. Jakob, M.,
Rose, R. L.,
Spielman, M. "Heat Transfer from an Air Jet to a
Plane Plate with Entrainment of
Water Vapor from the Environment",
Transactions of the ASME, volume 72,
page 859 (1950).
15. Colburn, A. P. "A Method of Correlating Forced
Convection Heat Transfer Data and
a Comparison with Fluid Friction",
Transactions of the A. I. Ch. E.,
volume 29, page 174 (1933).
16. Myers, G. E.,
Schauer, J. J.,
Eustis, R. H. "Heat Transfer to Plane Turbulent
Wall Jets", Journal of Heat Transfer
of the ASME, page 209, August (1963).
17. Akfirat, J. C. "Transfer of Heat from an Isothermal
Flat Plate to a Two-Dimensional Wall
Jet", ASME paper, page 274 (1966).
18. Hu, S. Y. "Heat Transfer in a Two-Dimensional
Wall Jet", University of Windsor,
Department of Mechanical Engineering,
Master's Thesis (1968).
19. Schuh, H.,
Persson, B. "Heat Transfer on Circular Cylinders
Exposed to Free Jet Flow", International
Journal of Heat and Mass Transfer,
volume 7, page 1257 (1964).
20. Rao, K. S. "Heat Transfer in a Two-Dimensional
Jet Flow over an Isothermal Curved
Wall", University of Windsor,
Department of Mechanical Engineering,
Master's Thesis (1968).

21. Rajaratnam, N.,
Froelich, C. R. "Boundary Shear Stress in Turbulent
Boundary Layers on Smooth Boundaries",
Journal of the Royal Aeronautical
Society, volume 71, page 52 (1967).
22. Hottel, H. C.,
Kalitinsky, A. "Temperature Measurements in High
Velocity Air Streams", Journal of
Applied Mechanics, page A-25 (1945).
23. Dean, R. C. "Aerodynamic Measurements",
The M. I. T. Press (1953).
24. Neville, A. M.,
Kennedy, J. B. "Basic Statistical Methods for
Engineers and Scientists",
International Textbook Company (1964).
25. Sridhar, K.,
Turchyn, A. "Design, Construction and Instrumentation
of a Low Speed Tandem Cascade Wind
Tunnel", University of Windsor,
Department of Mechanical Engineering
(Unpublished) (1969).
26. Hsu, S. "Engineering Heat Transfer", page 257,
Van Nostrand, Princeton, New Jersey
(1963).

TABLE I

NO.	EQUIPMENT	MODEL/TYPE	MEASURING EQUIPMENT		MEASUREMENT	MANUFACTURER
			RANGE	ACCURACY		
1.	temperature potentiometer	Model 2745	0-400°F	0.25°F	wall temperature static temperature	Honeywell Inc., Philadelphia, Pa., U.S.A.
2.	thermocouple ice point reference chamber	Model 136A		±0.02°F	ice point reference for temperature measurement	Thermoelectric Ltd. Brampton, Ontario.
3.	sloping manometer	alcohol filled, slopes 1:1, 1:2, 1:5, 1:10, 1:25	0-200mm	0.5mm (1:1 slope)	total pressure	Wilhelm Lambrecht, West Germany.
4.	pitot probe	flattened stainless steel hypodermic tubing			total pressure	Central Research Shop, University of Windsor.
5.	temperature probe	TA-12-c/c- 36-A-1-F bare thermocouple	0-400°F	0.5°F	static temperature	United Sensor and Control Corp., Watertown, Mass., U.S.A.
6.	precision potentiometer	Model 2779 microvolt	0-2111.0 μv.	±(0.02% of reading +0.02 μv)	heat flow rate	Honeywell, Denver, Colo., U.S.A.
7.	guarded null detector	Model 3990 microvolt	±0.1 μvFS to ±100mvFS	-5% +0.007 μv of FS range	null reading of precision potentiometer	Honeywell, Denver, Colo., U.S.A.
8.	heat flow sensors	Part No. 20453 micro-foil type	-300 to +400°F	1 $\frac{\text{BTU}}{\text{hrft}^2}$	heat flow rate	RDF Corp., Hudson, N.H., U.S.A.

TABLE II

ANGULAR POSITION θ , DEGREES	TRAVERSE LOCATIONS		
	DOWNSTREAM DISTANCE x, ft. (6.63" cyl.)	DOWNSTREAM DISTANCE x, ft. (4.00" cyl.)	DOWNSTREAM DISTANCE x, ft. (3.00" cyl.)
0	0	0	0
15	0.072	0.044	0.033
30	0.145	0.087	0.065
45	0.217	0.131	0.098
60	0.289	0.175	0.131
75	0.361	0.218	0.164
90	0.434	0.262	0.196

TABLE III
JET FLOW PARAMETERS
0.089 in. nozzle

θ DEGREES	LOCAL MAXIMUM VELOCITY u_m , ft./sec.									DISTANCE $y_m/2$, in.								
	6.63 in. cyl.			4.00 in. cyl.			3.00 in. cyl.			6.63" cyl.			4.00" cyl.			3.00" cyl.		
	CR	3OHR	6OHR	CR	3OHR	6OHR	CR	3OHR	6OHR	CR	3OHR	6OHR	CR	3OHR	6OHR	CR	3OHR	6OHR
15	127.7	126.9	128.5	139.8	140.7	141.5	149.7	149.6	148.4	.12	.12	.12	.09	.10	.10	.08	.09	.09
30	83.4	86.9	87.9	105.8	107.5	108.3	126.9	126.7	127.4	.23	.24	.24	.15	.15	.14	.11	.12	.12
45	66.1	69.7	70.0	85.3	85.4	86.0	95.1	102.1	102.4	.32	.37	.36	.22	.22	.21	.17	.17	.17
60	51.8	57.7	55.8	72.2	72.4	72.9	78.3	83.4	84.1	.40	.55	.54	.30	.29	.28	.22	.23	.23
75	42.2	48.1	48.0	59.4	59.2	59.2	68.1	69.2	69.4	.51	.72	.70	.36	.35	.35	.28	.29	.29
90	35.8	39.3	38.1	49.4	49.2	48.9	56.1	57.3	57.3	.64	.91	.93	.43	.42	.38	.33	.34	.33

LEGEND: CR - COLD RUN
 3OHR - HOT RUN - 30°F NOMINAL TEMP. DIFF.
 6OHR - HOT RUN - 60°F NOMINAL TEMP. DIFF.

TABLE IV
JET FLOW PARAMETERS

0.132 in. nozzle

θ DEGREES	LOCAL MAXIMUM VELOCITY u _m , ft./sec.									DISTANCE y _m /2, in.								
	6.63 in. cyl.			4.00 in. cyl.			3.00 in. cyl.			6.63" cyl.			4.00" cyl.			3.00" cyl.		
	CR	3OHR	6OHR	CR	3OHR	6OHR	CR	3OHR	6OHR	CR	3OHR	6OHR	CR	3OHR	6OHR	CR	3OHR	6OHR
15	145.1	142.3	142.8	151.5	151.8	152.7	153.1	155.3	156.5	.16	.16	.16	.13	.14	.13	.12	.13	.13
30	106.6	104.5	105.2	133.3	131.8	133.8	142.4	143.2	145.4	.26	.27	.27	.17	.18	.17	.14	.15	.15
45	82.9	83.6	83.4	103.9	103.2	105.0	122.4	123.6	125.2	.40	.41	.41	.25	.26	.26	.19	.20	.20
60	71.3	71.6	71.8	84.8	85.0	85.4	95.0	101.9	103.2	.51	.56	.54	.36	.35	.36	.26	.27	.27
75	60.2	60.1	60.1	75.0	75.6	75.8	79.9	87.5	88.9	.66	.74	.71	.46	.46	.46	.33	.34	.34
90	51.0	49.9	51.7	65.8	64.5	64.8	71.7	74.0	74.4	.83	.88	.87	.59	.57	.60	.38	.41	.41

LEGEND: CR - COLD RUN

3OHR - HOT RUN - 30°F NOMINAL TEMP. DIFF.

6OHR - HOT RUN - 60°F NOMINAL TEMP. DIFF.

TABLE V
JET FLOW PARAMETERS
 0.250 in. nozzle

θ DEGREES	LOCAL MAXIMUM VELOCITY u_m , ft./sec.												DISTANCE $y_m/2$, in.					
	6.63 in. cyl.		4.00 in. cyl.		3.00 in. cyl.		6.63 in. cyl.		4.00 in. cyl.		3.00 in. cyl.		6.63 in. cyl.		4.00 in. cyl.		3.00 in. cyl.	
	CR	30HR	60HR	CR	30HR	60HR	CR	30HR	60HR	CR	30HR	60HR	CR	30HR	60HR	CR	30HR	60HR
15	150.1	154.3	154.2	153.6	153.6	153.7	154.8	155.4	155.1	154.8	155.1	154.4	154.8	155.1	154.4	154.8	155.1	154.4
30	135.5	140.6	139.9	152.5	152.1	152.3	145.8	142.9	142.8	151.7	151.9	151.0	145.4	144.3	142.7	133.7	131.2	128.8
45	108.6	119.9	112.7	131.9	126.8	127.6	107.9	105.1	105.1	93.1	90.9	90.5	111.3	108.8	106.9	111.3	108.8	106.9
60	89.1	95.3	94.9	107.9	105.1	105.1	107.9	105.1	105.1	93.1	90.9	90.5	111.3	108.8	106.9	111.3	108.8	106.9
75	75.6	81.4	80.4	107.9	105.1	105.1	107.9	105.1	105.1	93.1	90.9	90.5	111.3	108.8	106.9	111.3	108.8	106.9
90	66.7	73.2	72.8	107.9	105.1	105.1	107.9	105.1	105.1	93.1	90.9	90.5	111.3	108.8	106.9	111.3	108.8	106.9

LEGEND: CR - COLD RUN

30HR - HOT RUN - 30°F NOMINAL TEMP. DIFF.

60HR - HOT RUN - 60°F NOMINAL TEMP. DIFF.

TABLE VI
COMPARISON OF TEMPERATURE
PROFILE CORRELATIONS

	6.63 in. cyl.		4.00 in. cyl.		3.00 in. cyl.	
	30HR	60HR	30HR	60HR	30HR	60HR
TEMP. → DIFF. →	.089	.132	.250	.089	.132	.250
NOZZLE SIZE →	.089	.132	.250	.089	.132	.250
K ₁ →	.65	.65	.53	.81	.80	.73
K ₂ →	.080	.12	.19	.048	.065	.11
K ₃ →	.065	.060	.11	.026	.031	.046
	.089	.132	.250	.089	.132	.250
	.80	.75	.53	.87	.82	.75
	.11	.15	.32	.062	.076	.11
	.015	.010	.12	.003	.022	.047
	.011	.006	.021			

$$\frac{T_w - T}{T_w - T_a} = K_1 \left(\frac{y}{y_m/2} \right)^{K_2} \left(\frac{x}{t} \right)^{K_3}$$

TABLE VII

HEAT TRANSFER(NUSSELT NUMBERS - $(Nu)_t$)
(COLBURN ANALOGY)

NOZZLE WIDTH, in.	0.089		0.132		0.250	
	30HR	60HR	30HR	60HR	30HR	60HR
NOZZLE REYNOLDS NUMBER	6530		9740		18400	
TEMP. DIFF.	0.089		0.132		0.250	
CYLINDER SIZE	6530		9740		18400	
θ , DEGREES	6530		9740		18400	
15	12.8	15.9	18.8	13.0	16.1	18.7
30	7.6	10.9	14.5	7.7	11.0	14.7
45	4.7	7.3	9.8	4.7	7.4	9.7
60	3.3	5.0	6.8	3.1	5.1	6.9
75	2.1	3.5	5.0	2.1	3.5	5.0
90	1.3	2.5	3.2	1.3	2.5	3.2
	6.63	4.00	3.00	6.63	4.00	3.00
	12.8	15.9	18.8	23.1	25.8	28.3
	7.6	10.9	14.5	15.1	20.6	25.0
	4.7	7.3	9.8	10.2	14.5	17.6
	3.3	5.0	6.8	6.7	10.4	12.8
	2.1	3.5	5.0	4.8	7.7	10.0
	1.3	2.5	3.2	3.2	5.5	7.2
	6.63	4.00	3.00	6.63	4.00	3.00
	37.6	43.0	46.0	23.4	26.8	30.1
	35.0	40.0	44.6	15.3	21.3	25.0
	27.6	36.9	43.1	10.1	14.9	17.7
	21.5	28.6	36.0	6.8	10.3	12.9
	17.0	23.6	32.3	4.8	7.6	10.4
	12.9	19.6	24.7	3.4	5.6	7.2
	6.63	4.00	3.00	6.63	4.00	3.00
	39.4	44.0	48.5	39.4	44.0	48.5
	35.6	40.5	43.6	35.6	40.5	43.6
	27.1	37.9	39.3	27.1	37.9	39.3
	21.1	30.6	34.8	21.1	30.6	34.8
	16.7	24.2	29.1	16.7	24.2	29.1
	12.5	19.8	23.1	12.5	19.8	23.1

TABLE VIII
HEAT TRANSFER
 (NUSSELT NUMBERS - $(Nu)_t$)
 (INTEGRATION METHOD)

	0.089	0.132	0.250
→ NOZZLE WIDTH, in.			
→ NOZZLE REYNOLDS NUMBER	6530	9740	18400
→ TEMP. DIFF.	30HR	30HR	30HR
→ CYLINDER SIZE			
→ <u>θ, DEGREES</u>			
15	340.5	1333.5	65.2
30	241.7	1207.1	44.1
45	224.2	2160.2	42.1
60	224.2	88.5	49.9
75	226.0	80.5	80.5
90	240.2	70.8	3.5
	<u>6.630</u>	<u>6.63</u>	<u>6.63</u>
	<u>4.00</u>	<u>4.00</u>	<u>4.00</u>
	<u>3.00</u>	<u>3.00</u>	<u>3.00</u>
	82.8	167.1	-151.2
	50.0	99.8	-74.8
	37.4	74.5	-50.1
	29.8	58.8	-38.3
	25.2	50.1	-31.0
	22.3	44.4	-26.1
			-27.3
			-13.7
			-9.1
			-6.8
			-5.5
			-4.6

TABLE IX

HEAT TRANSFER
CORRELATIONS

(INTEGRATION METHOD)

	<u>6.63 in. cyl.</u>	<u>4.00 in. cyl.</u>	<u>3.00 in. cyl.</u>
c_1	0.017	0.058	0.048
c_2	0.80	0.80	0.80
c_3	-0.0083	0.49	-0.26

$$(\text{Nu})_t = c_1 (\text{Re})_t^{c_2} (x/t)^{-c_3}$$

TABLE X
COMPARISON OF HEAT
TRANSFER CORRELATIONS

	6.63 in. cyl.	4.00 in. cyl.	3.00 in. cyl.	Akfirat (Ref. 17)	Hu (Ref. 18)	Rao (Ref. 20)
C_1	0.12 \pm 0.01	0.12 \pm 0.02	0.11 \pm 0.02	0.097	0.071	0.71
C_2	0.80	0.80	0.80	0.80	0.80	0.80
C_3	1.03 \pm 0.04	1.06 \pm 0.07	1.04 \pm 0.05	0.60	0.54	0.61

$$(Nu)_t = C_1 (Re)_t^{C_2} (x/t)^{-C_3}$$

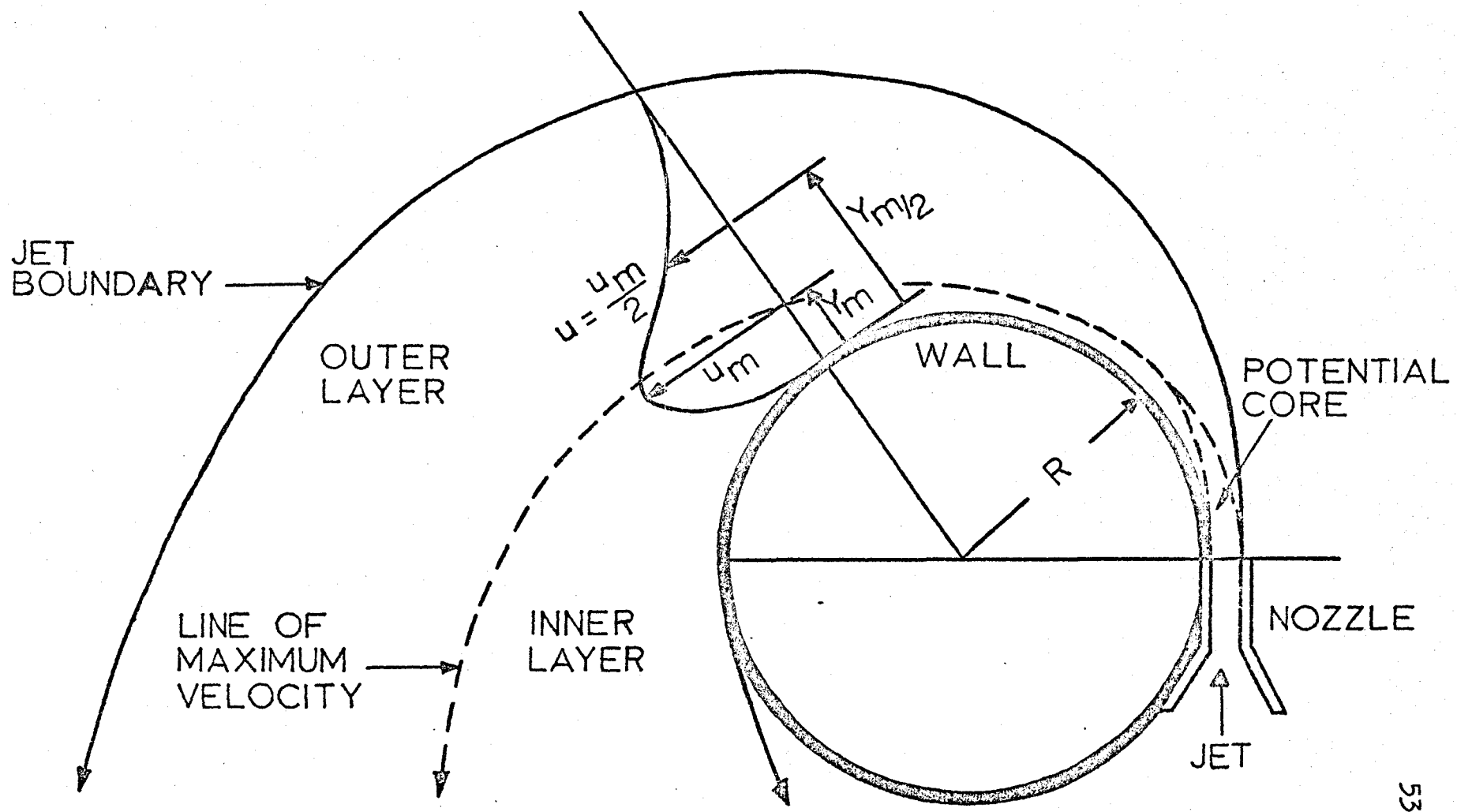
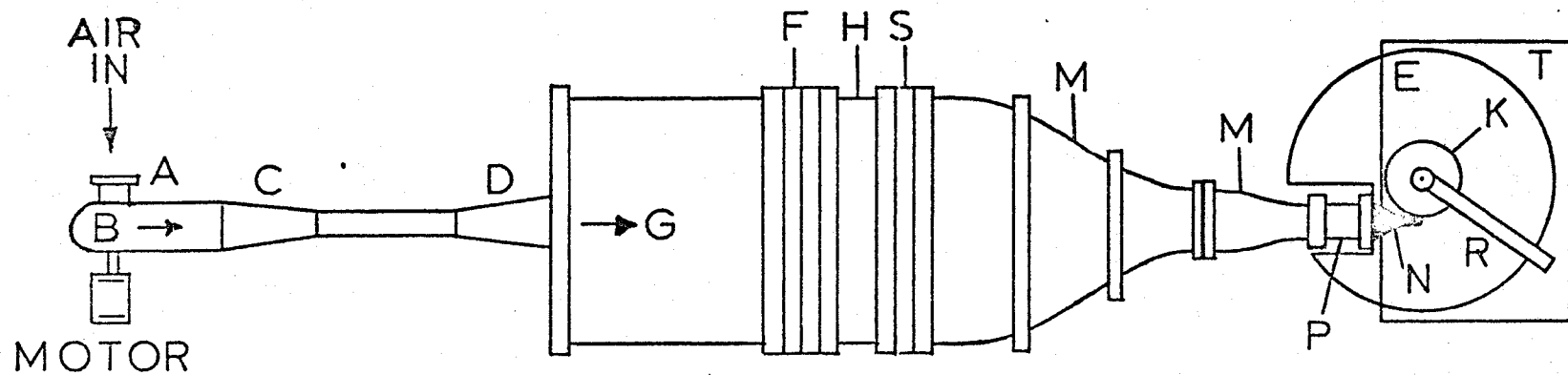


Fig. 1 CURVED WALL JET NOMENCLATURE



A - BLAST GATE

B - BLOWER

C - BLEEDING SECTION

D - DIFFUSER SECTION

E - END-PLATES

F - FILTER SECTION

G - PLENUM CHAMBER

H - HONEYCOMB SECTION

K - TEST CYLINDER

M - CONTRACTION SECTION

N - NOZZLE

P - PLEXIGLAS DUCT

R - TRAVERSING MECHANISM

AND PROBES

S - SCREENS

T - SUPPORTING TABLE

Fig. 2 SCHEMATIC DIAGRAM OF TEST FACILITIES

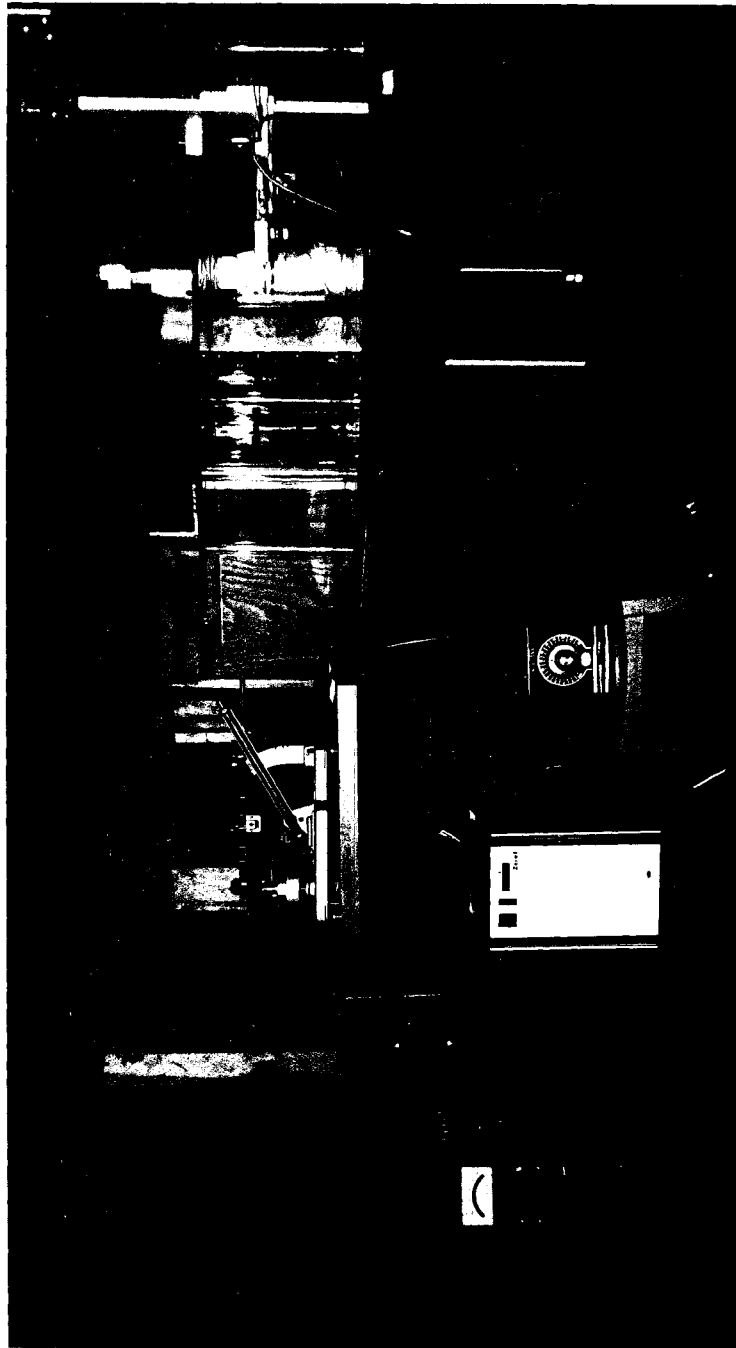


FIG. 3 TEST FACILITIES

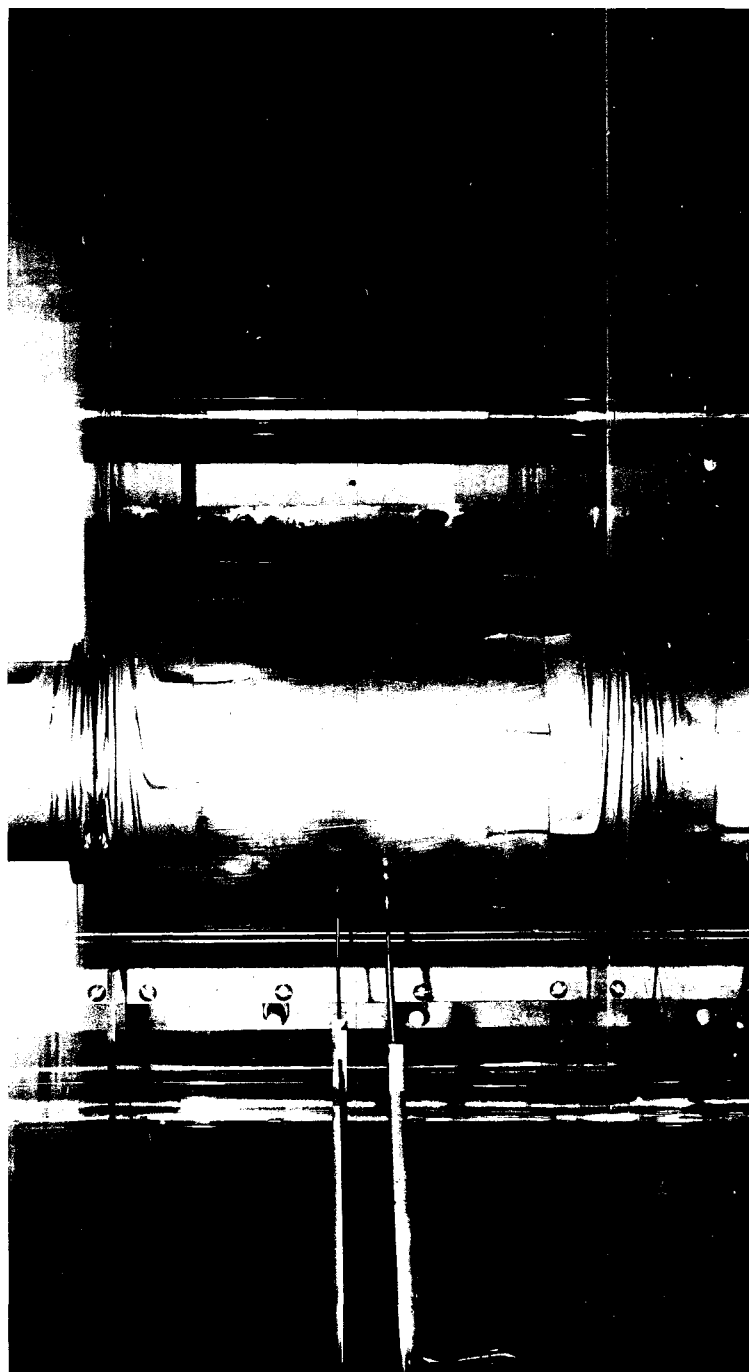
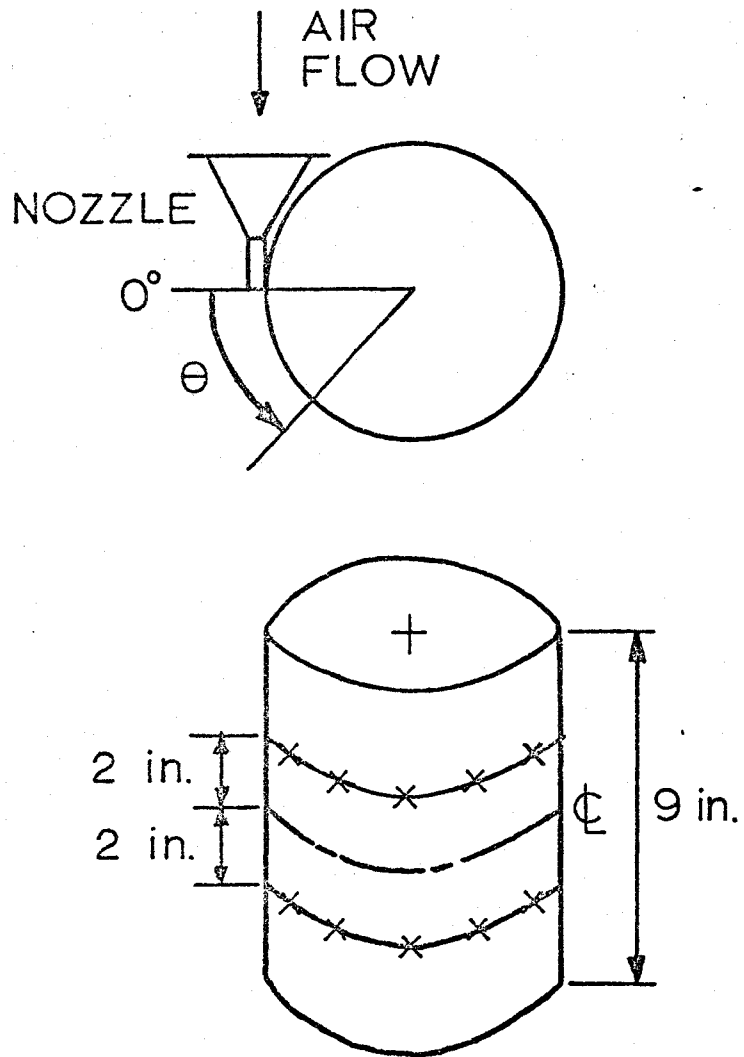


FIG. 4 TEST SURFACE AND TRAVERSING MECHANISM



COPPER-CONSTANTAN
THERMOCOUPLES
EMBEDDED IN
CYLINDER SURFACE AT:

- 1) 2 in. above ζ :
 $\theta = 15^\circ, 45^\circ, 75^\circ, 105^\circ, 135^\circ, 165^\circ$
- 2) 2 in. below ζ :
 $\theta = 30^\circ, 60^\circ, 90^\circ, 120^\circ, 150^\circ, 180^\circ$

HEAT FLOW
SENSORS AT:

$\theta = 30^\circ, 45^\circ, 60^\circ$

Fig. 5 LAYOUT OF TEST SURFACE

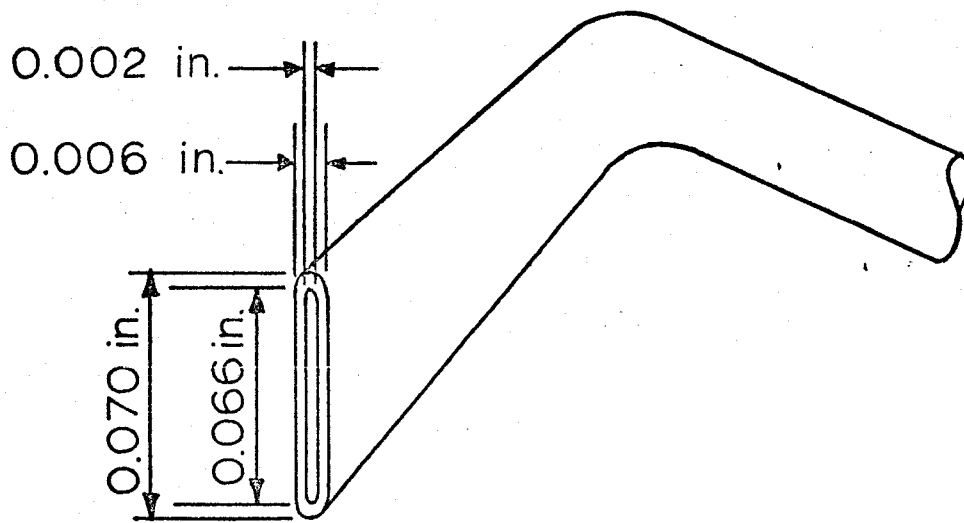
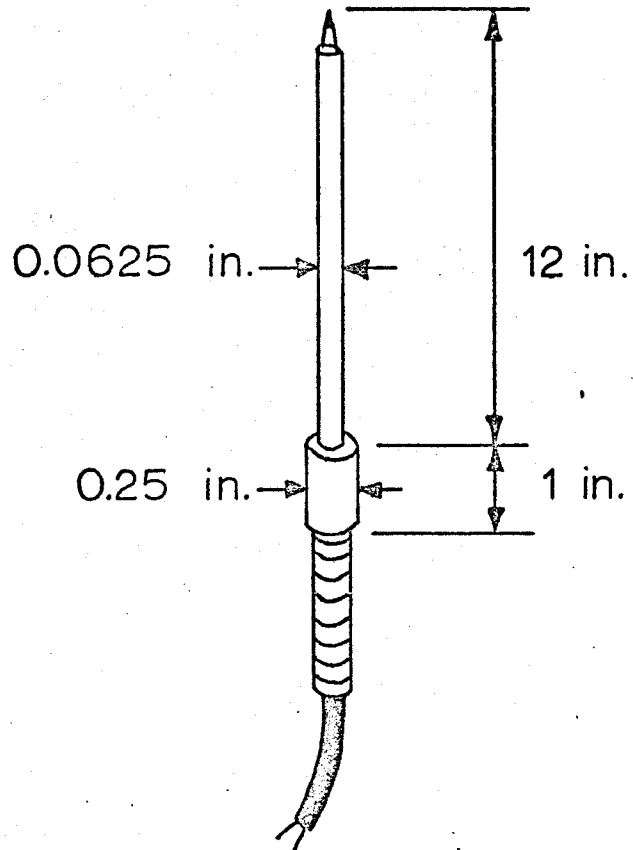


Fig. 6 TOTAL PRESSURE PROBE



TYPE: EXPOSED JUNCTION,
STAINLESS STEEL STEM

THERMOCOUPLE WIRE:
COPPER - CONSTANTAN

Fig. 7 TEMPERATURE PROBE

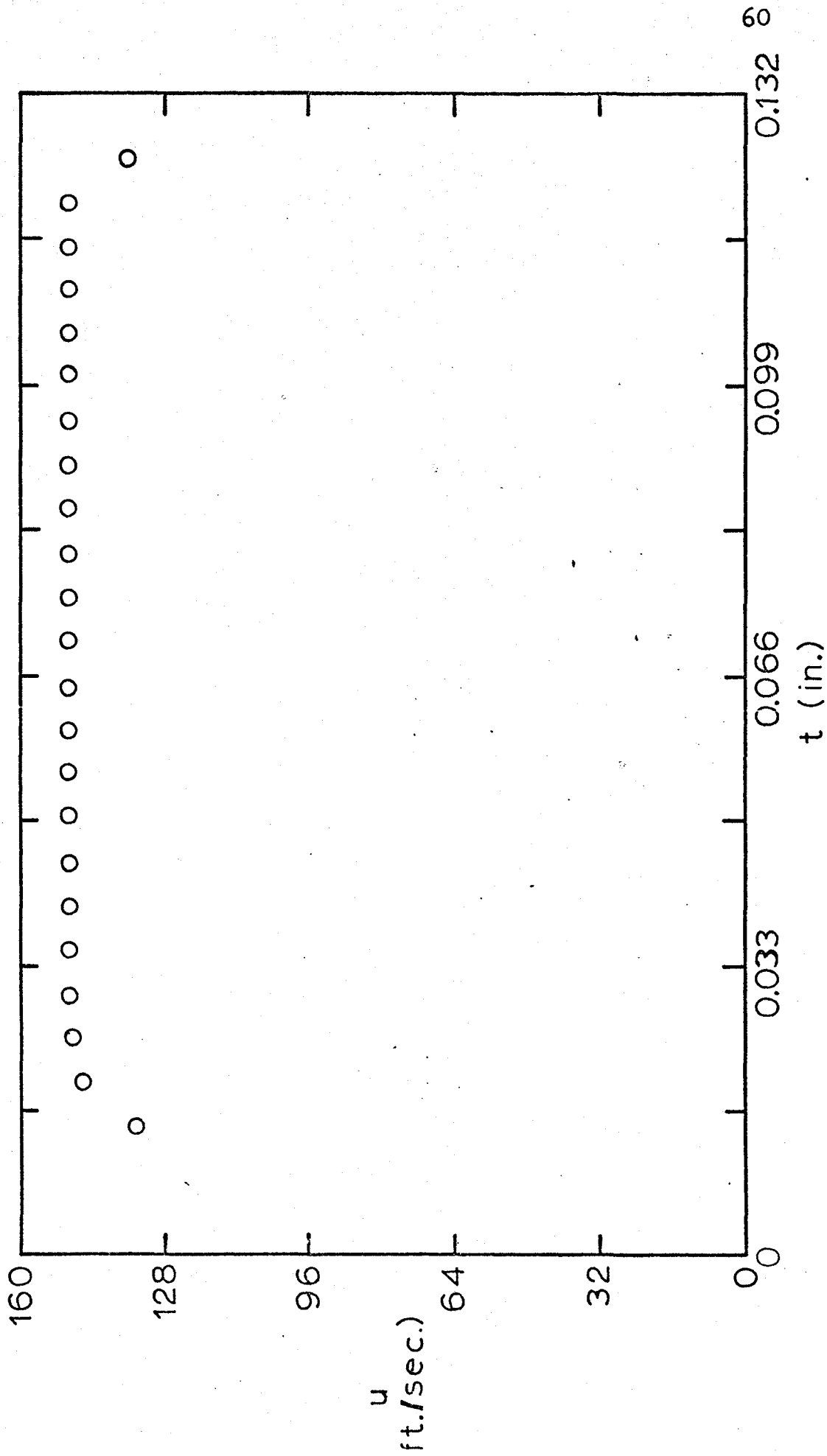


Fig. 8 VELOCITY DISTRIBUTION AT NOZZLE EXIT
0.132 in. nozzle

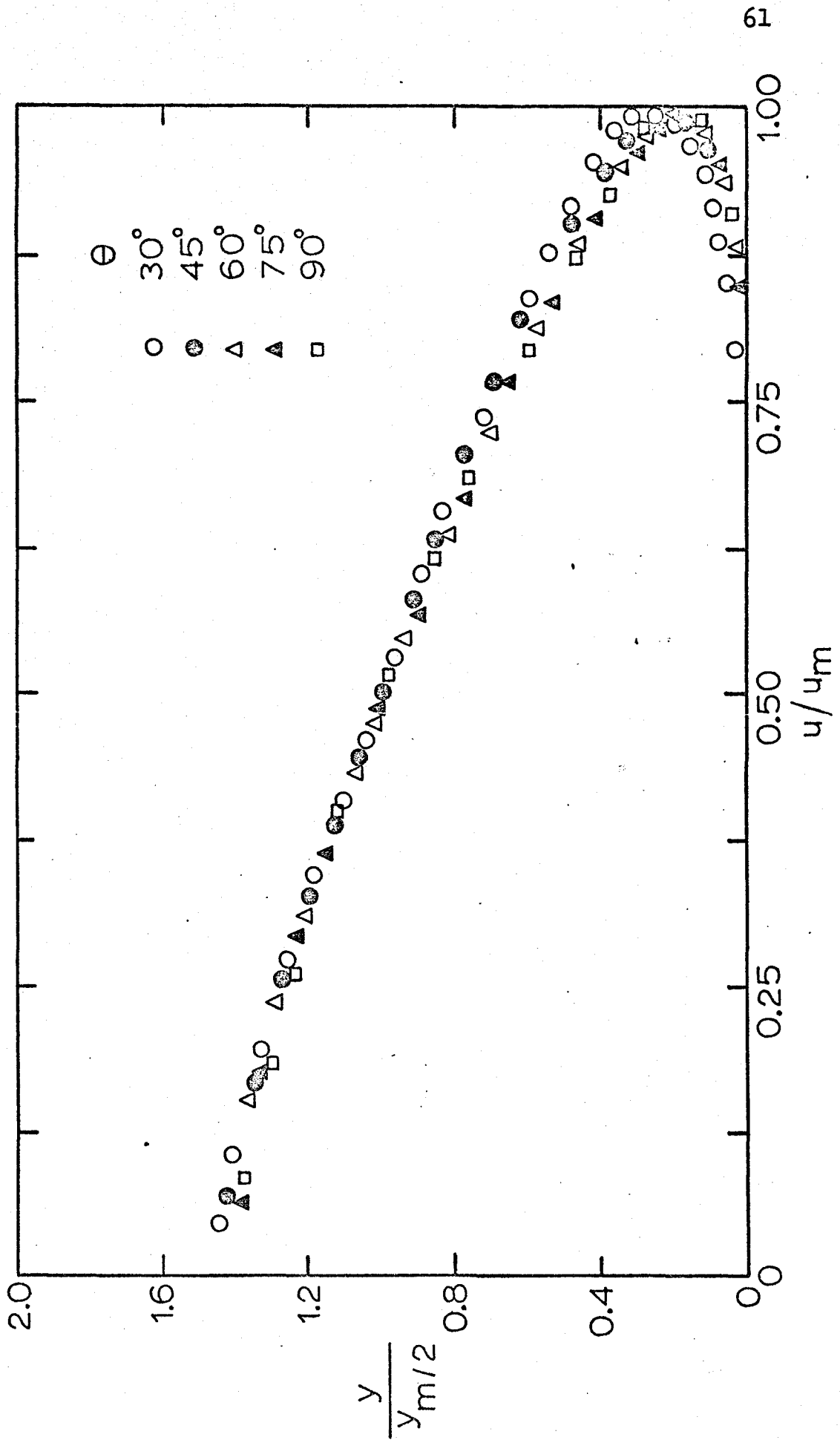


Fig. 9 NON-DIMENSIONAL VELOCITY PROFILES
6.63 in. cyl., 0.132 in. nozzle

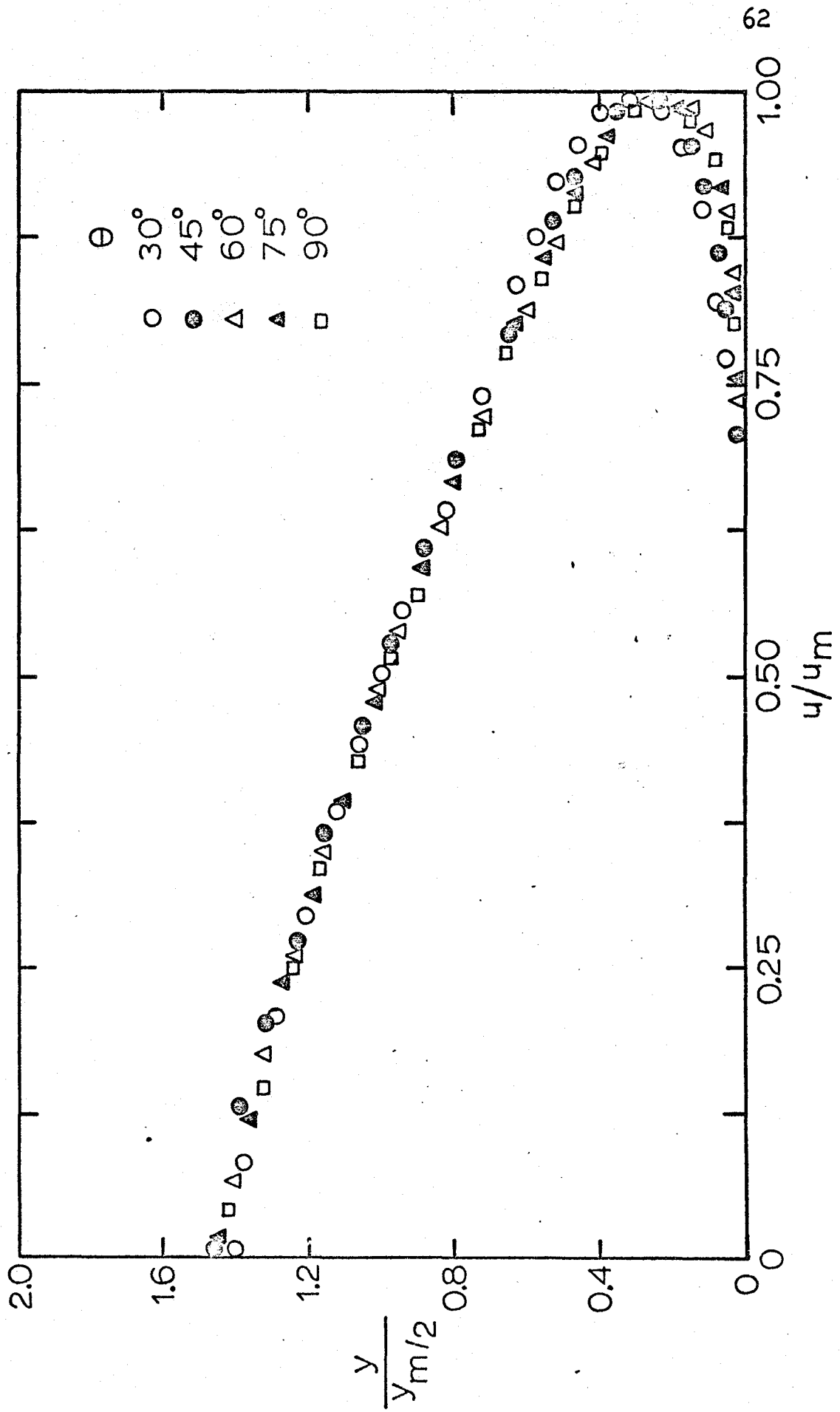


Fig. 10 NON-DIMENSIONAL VELOCITY PROFILES
4.00 in. cyl., 0.132 in. nozzle

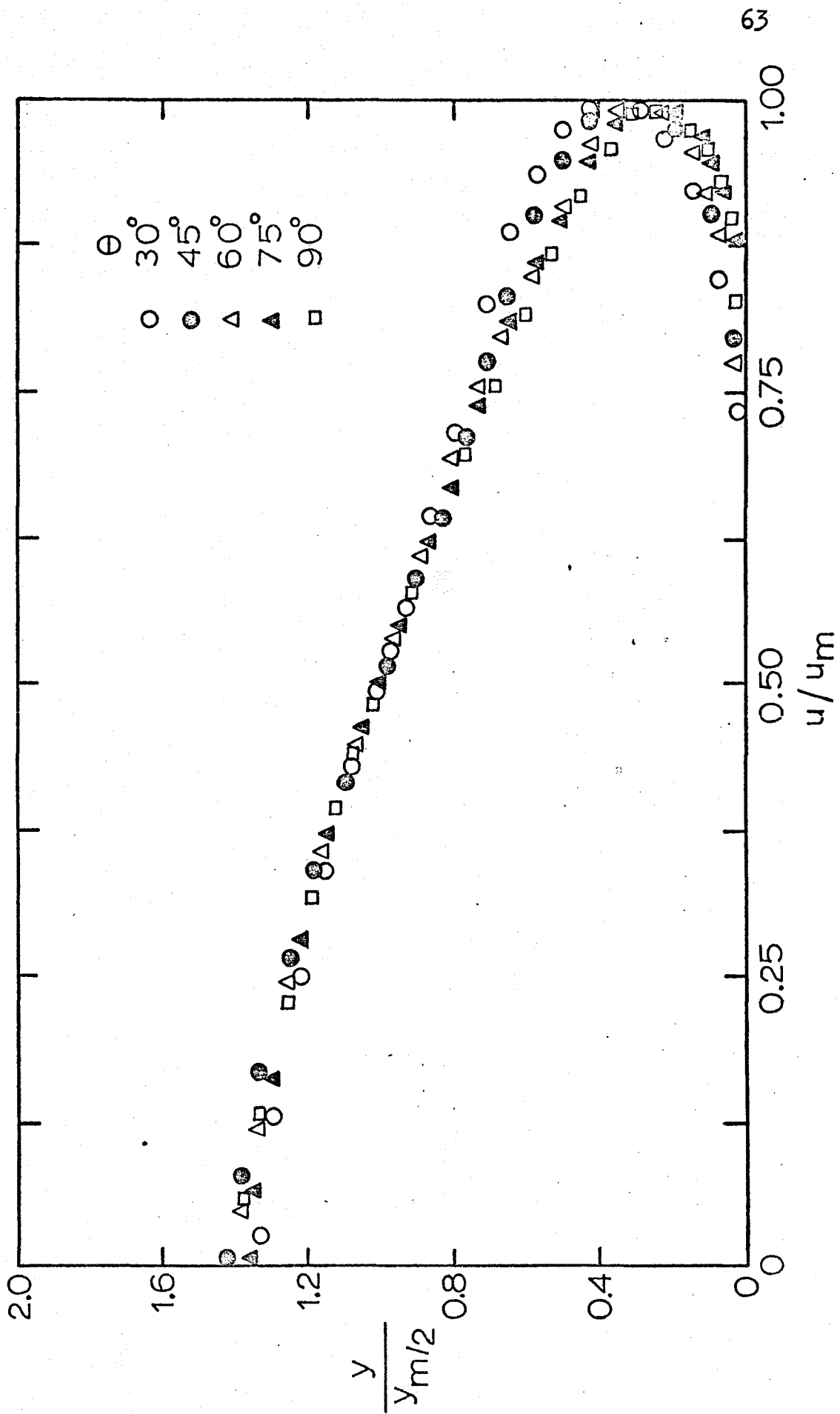


FIG. 11 NON-DIMENSIONAL VELOCITY PROFILES
 3.00 in. cyl., 0.132 in. nozzle

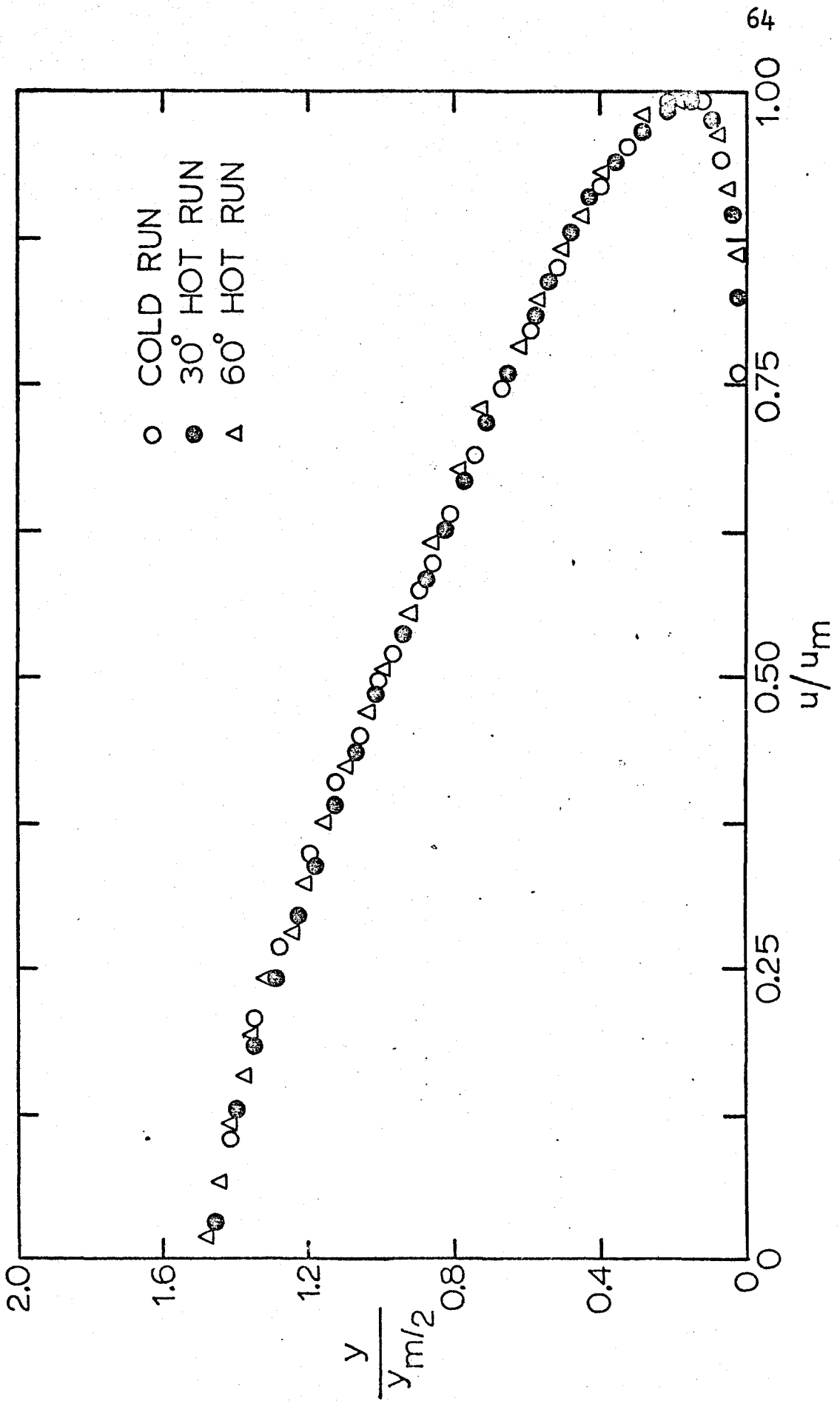


FIG. 12 COMPARISON OF VELOCITY PROFILES
 FOR HEATED AND UNHEATED WALLS
 6.63 in. cyl., 0.089 in. nozzle, $\theta = 60^\circ$

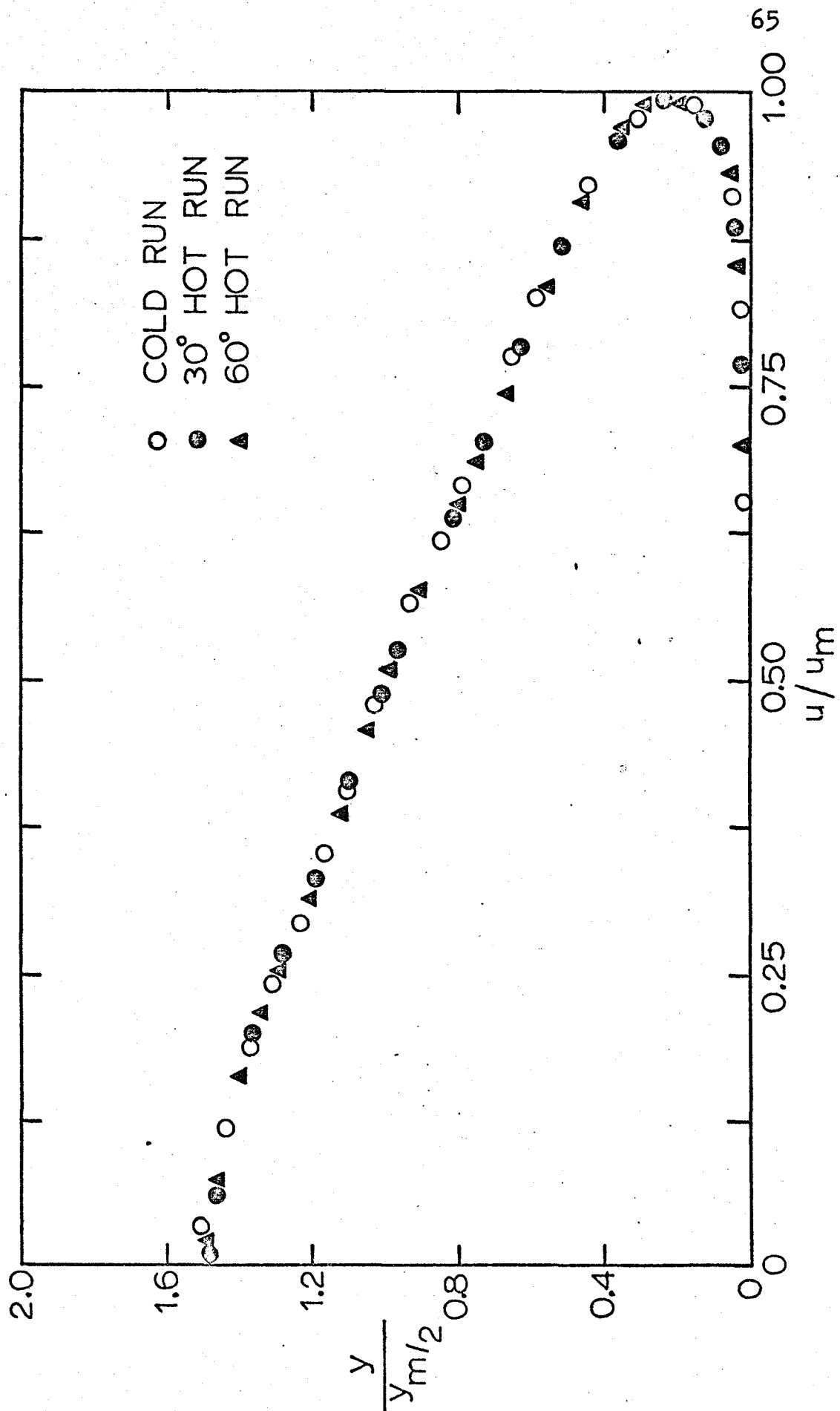


Fig. 13 COMPARISON OF VELOCITY PROFILES
 FOR HEATED AND UNHEATED WALLS
 3.00 in. cyl., 0.089 in. nozzle, $\theta = 60^\circ$

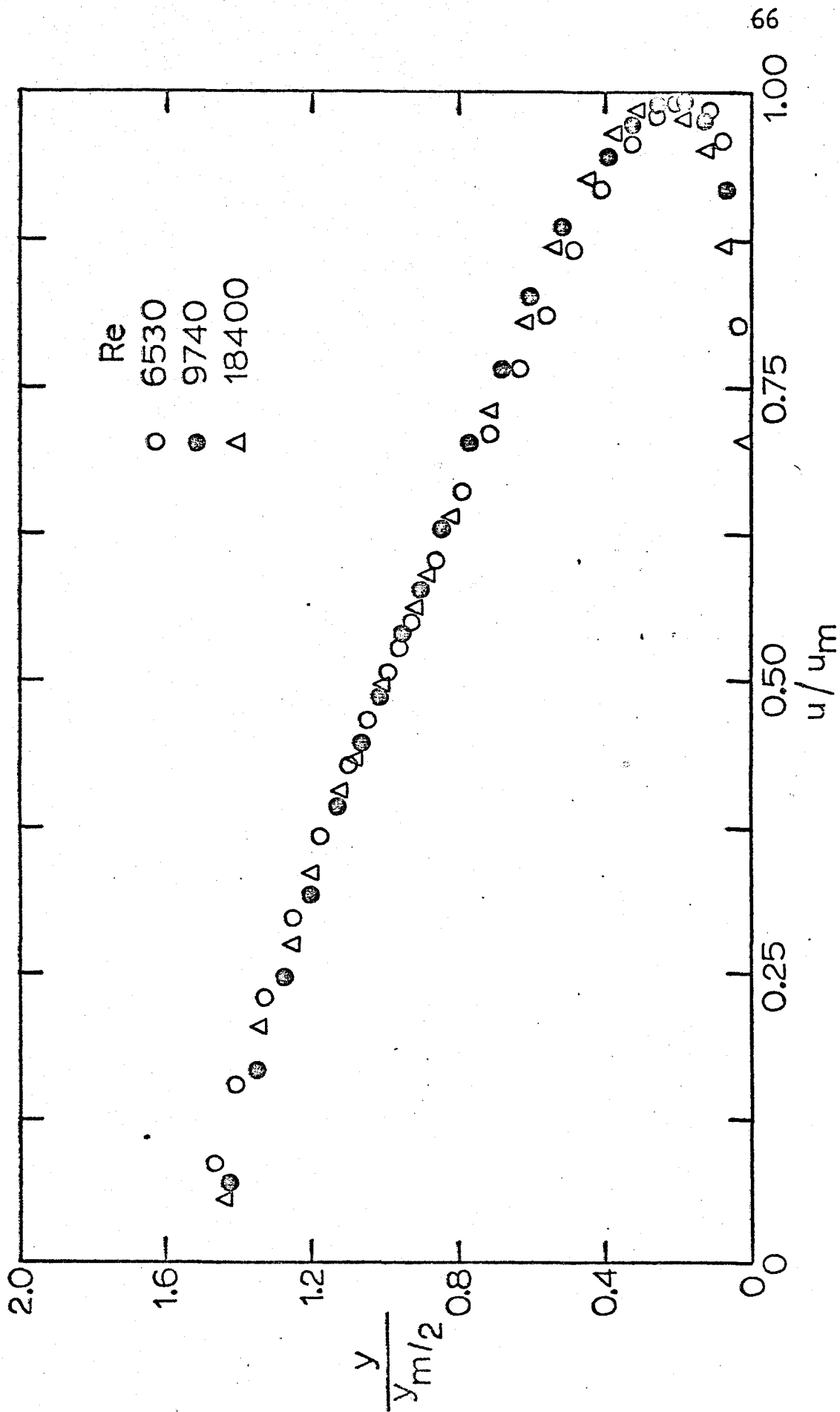


FIG. 14 EFFECT OF VARYING REYNOLDS NUMBER ON VELOCITY PROFILES
6.63 in. cyl., $\theta=45^\circ$

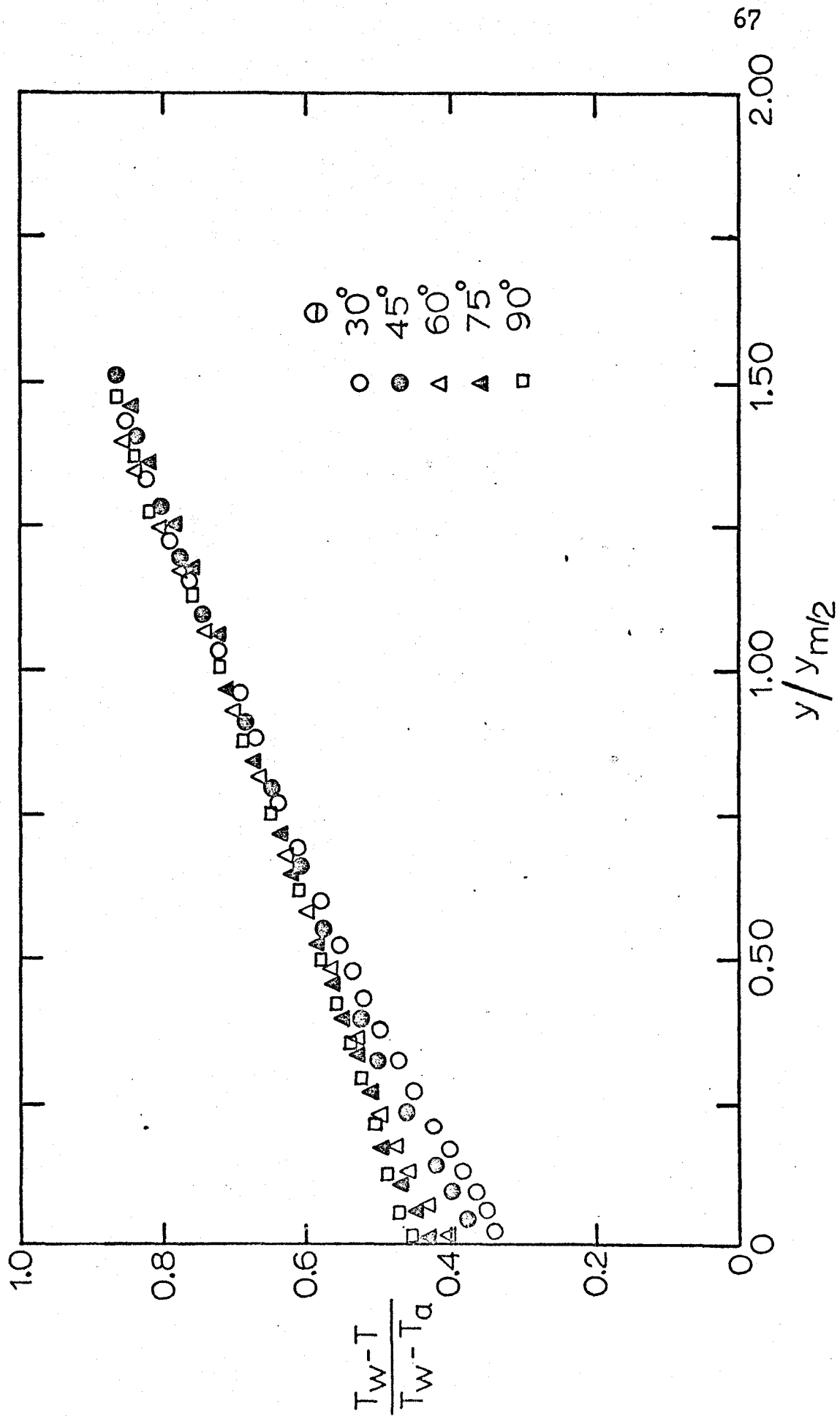


Fig. 15 NON-DIMENSIONAL TEMPERATURE PROFILES
 6.63 in. cyl., 0.250 in. nozzle, 30°F HOT RUN

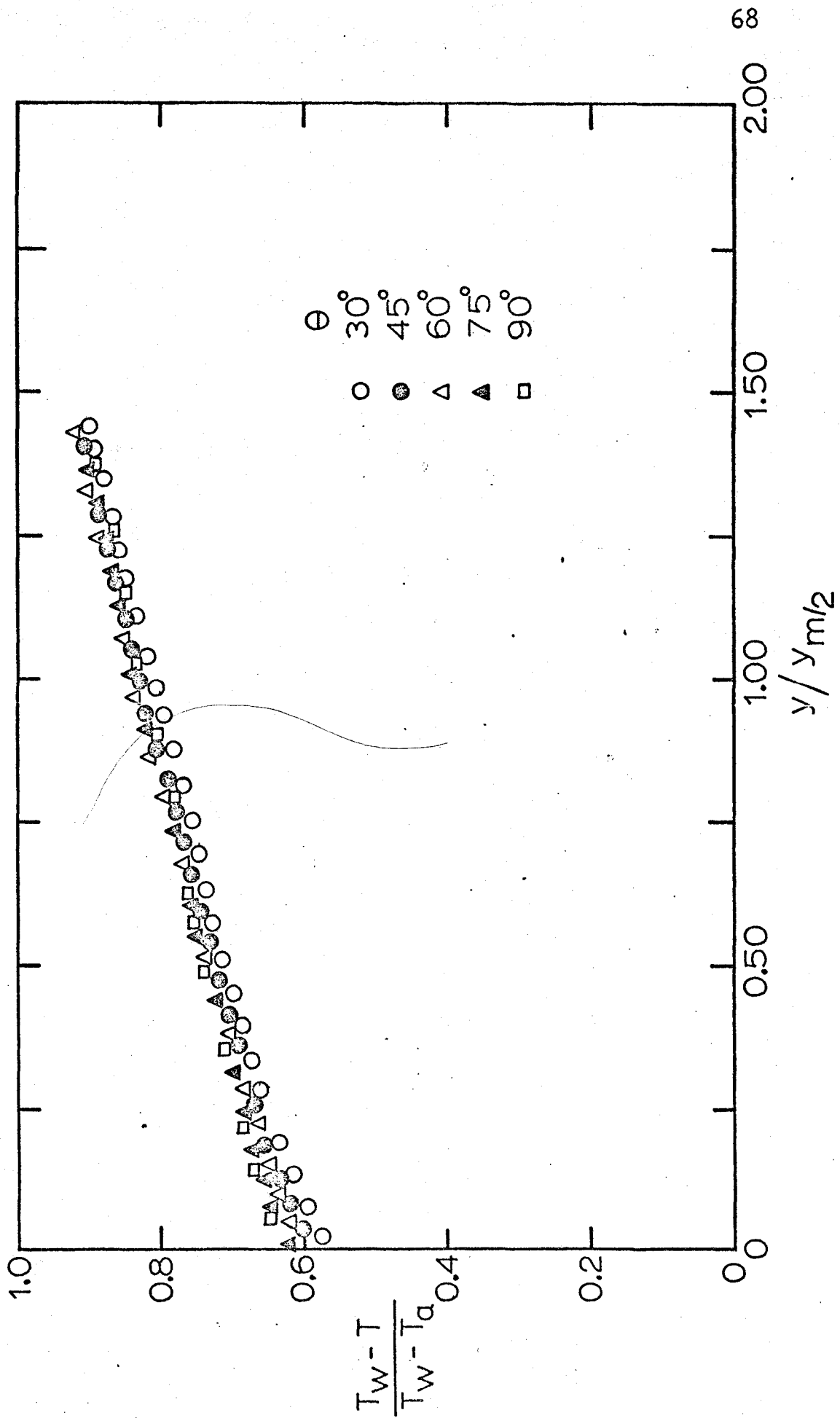


Fig. 16 NON-DIMENSIONAL TEMPERATURE PROFILES
 6.63 in. cyl., 0.250 in. nozzle, 60°F HOT RUN

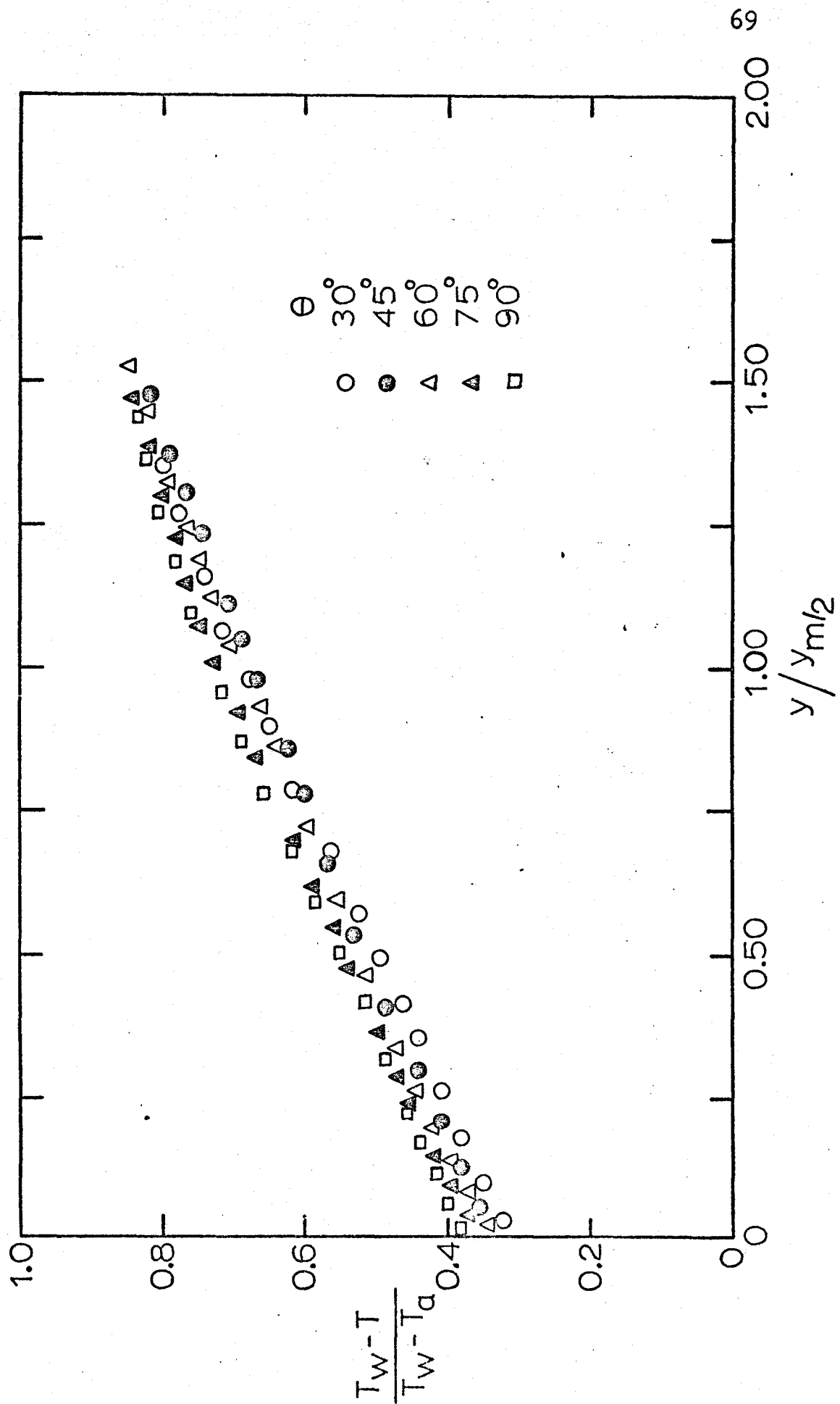


Fig. 17 NON-DIMENSIONAL TEMPERATURE PROFILES
 4.00 in. cyl., 0.250 in. nozzle, 30°F HOT RUN

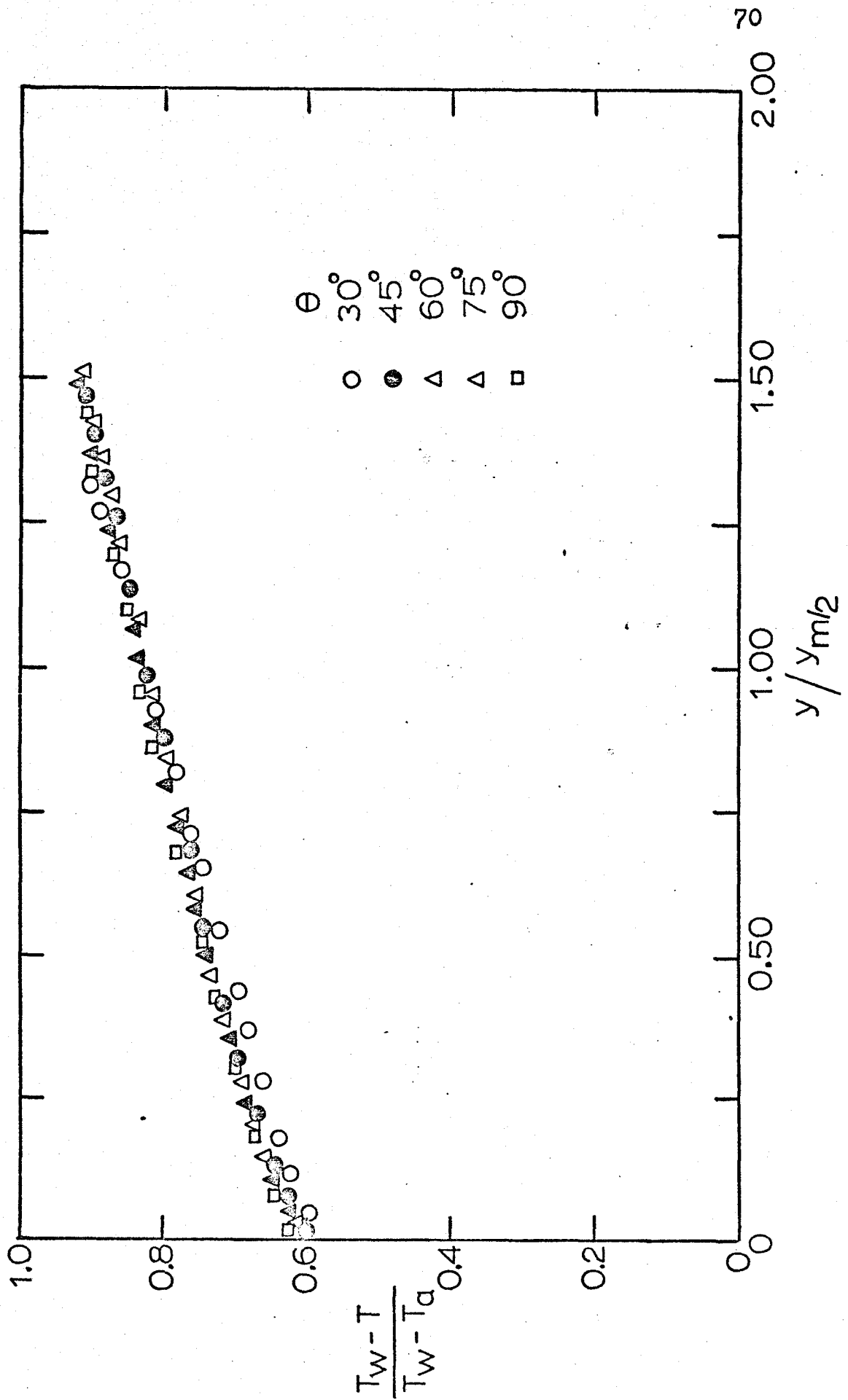


Fig. 18 NON-DIMENSIONAL TEMPERATURE PROFILES
 4.00 in. cyl., 0.250 in. nozzle, 60°F HOT RUN

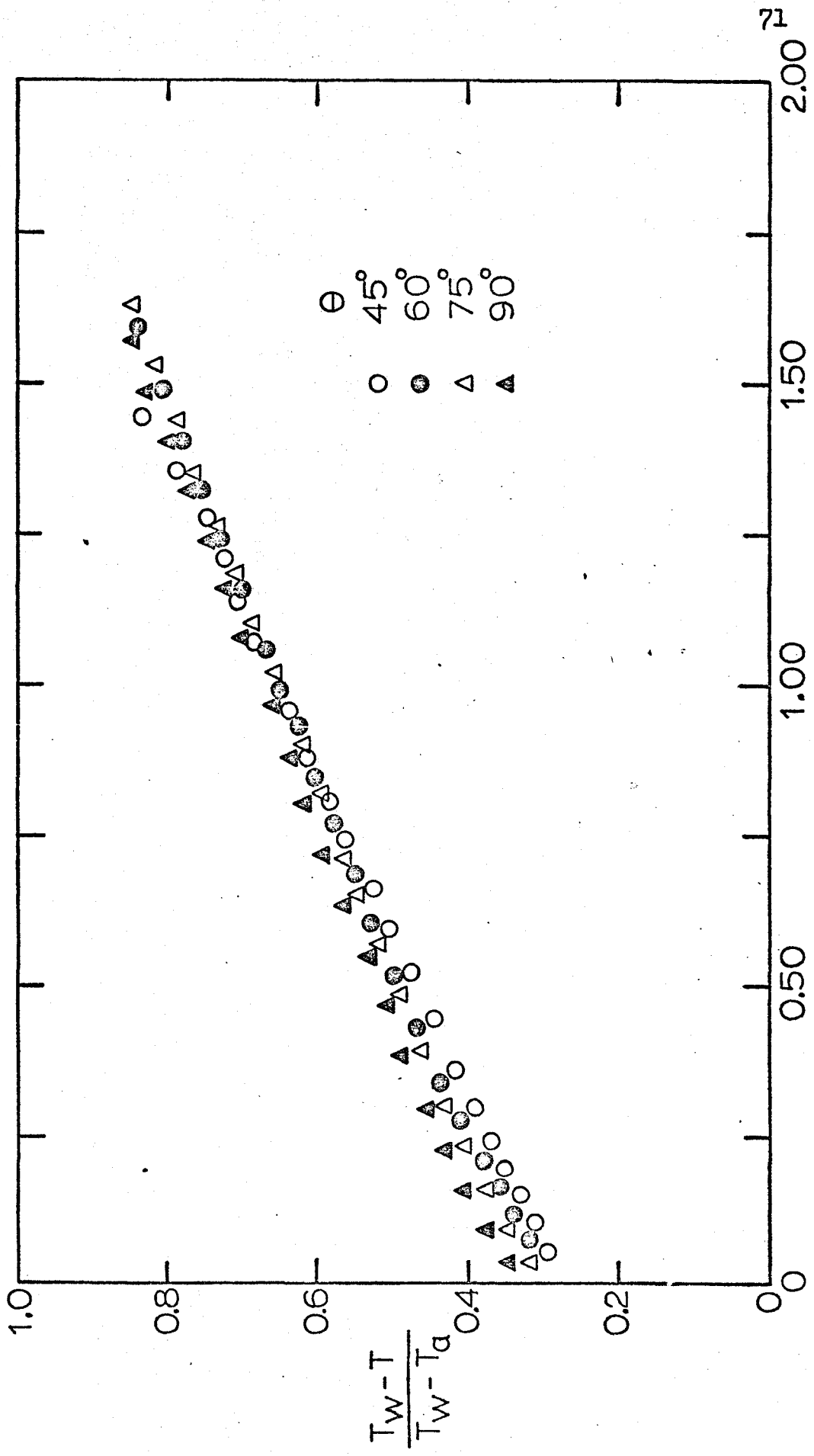


Fig. 19 NON-DIMENSIONAL TEMPERATURE PROFILES
 3.00 in. cyl., 0.250 in. nozzle, 30°F HOT RUN

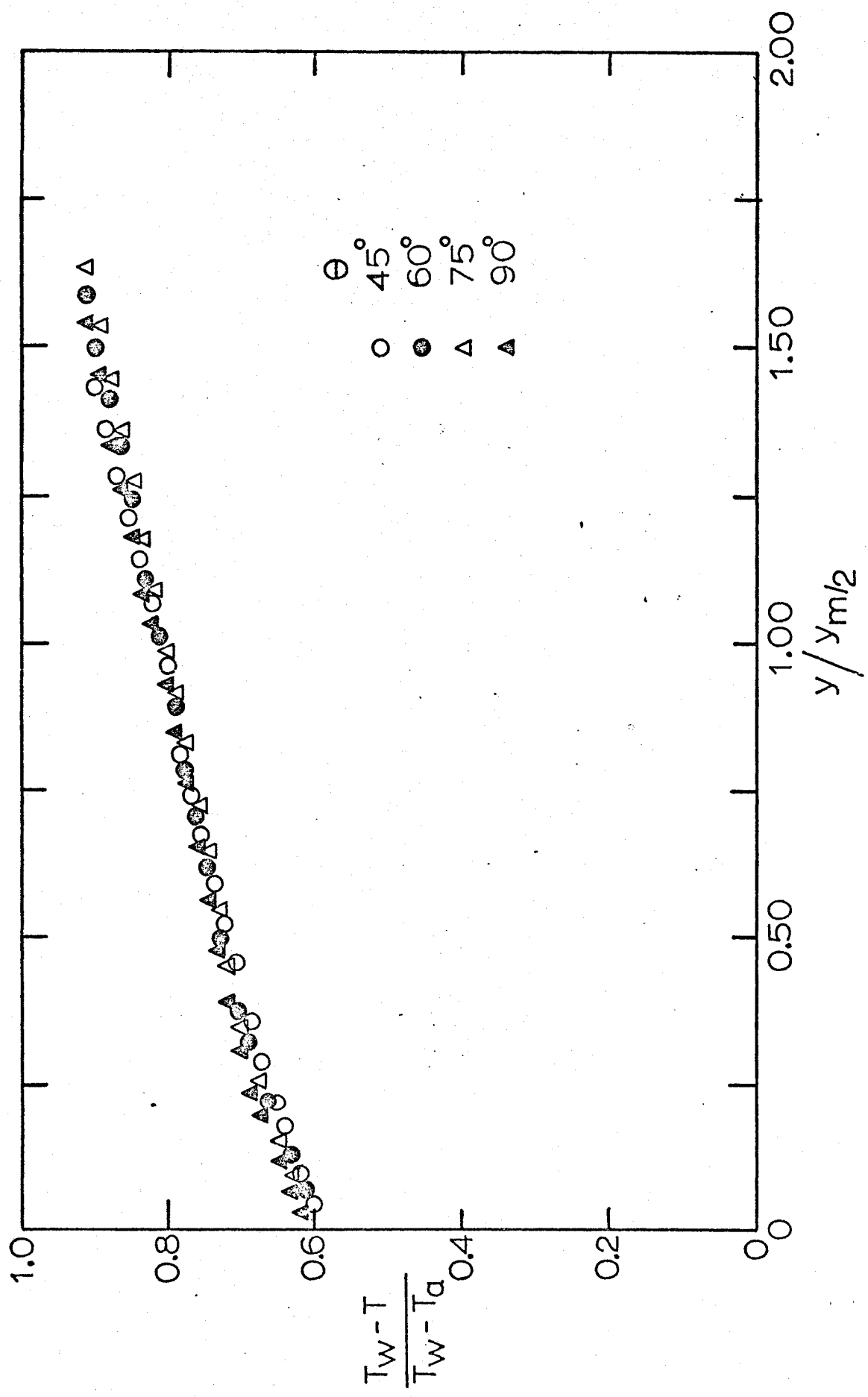


Fig. 20 NON-DIMENSIONAL TEMPERATURE PROFILES
3.00 in. cyl., 0.250 in. nozzle, 60°F HOT RUN

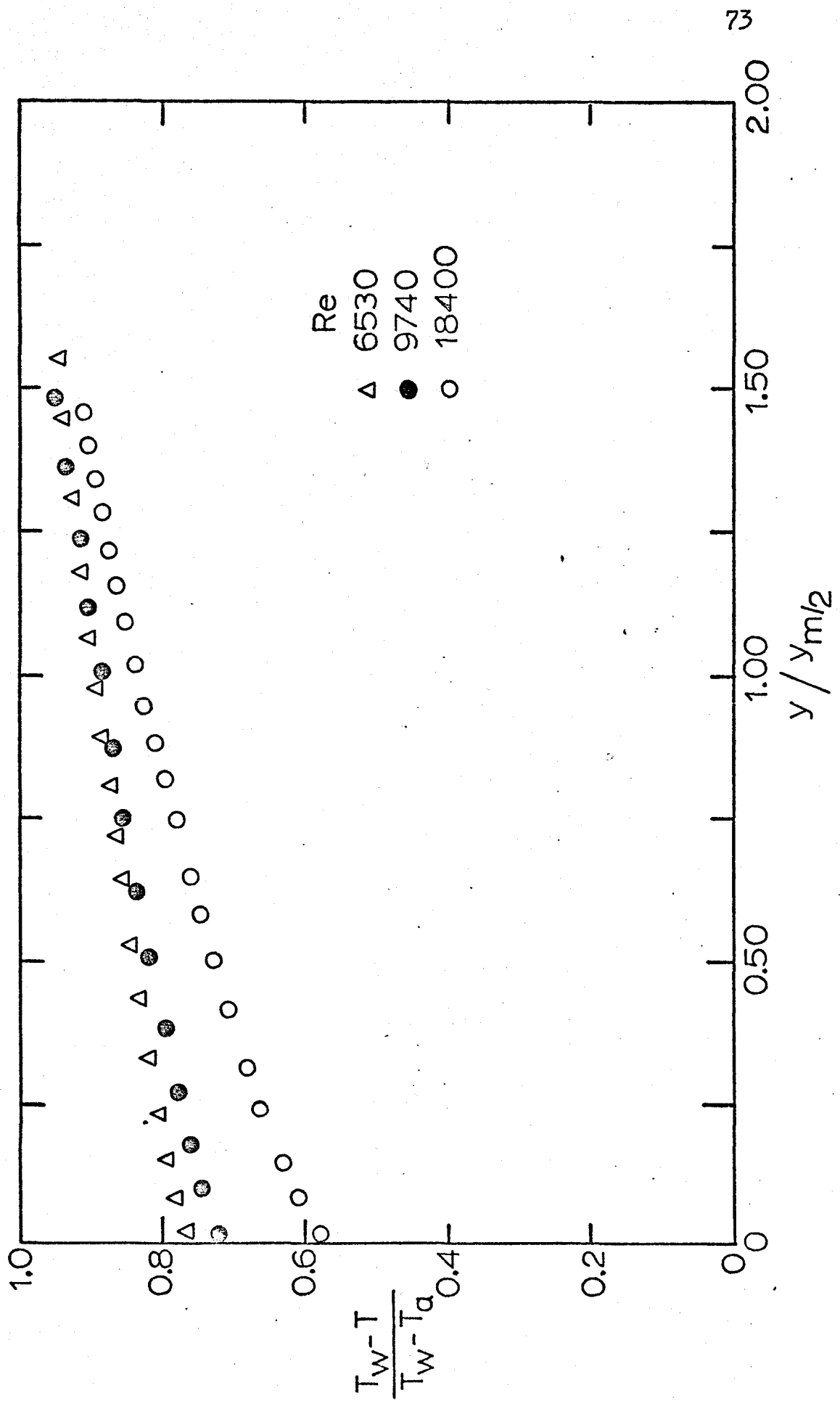


FIG. 21 EFFECT OF VARYING REYNOLDS NUMBER ON TEMPERATURE PROFILES
 6.63 in. cyl., 60°F HOT RUN, $\theta = 45^\circ$

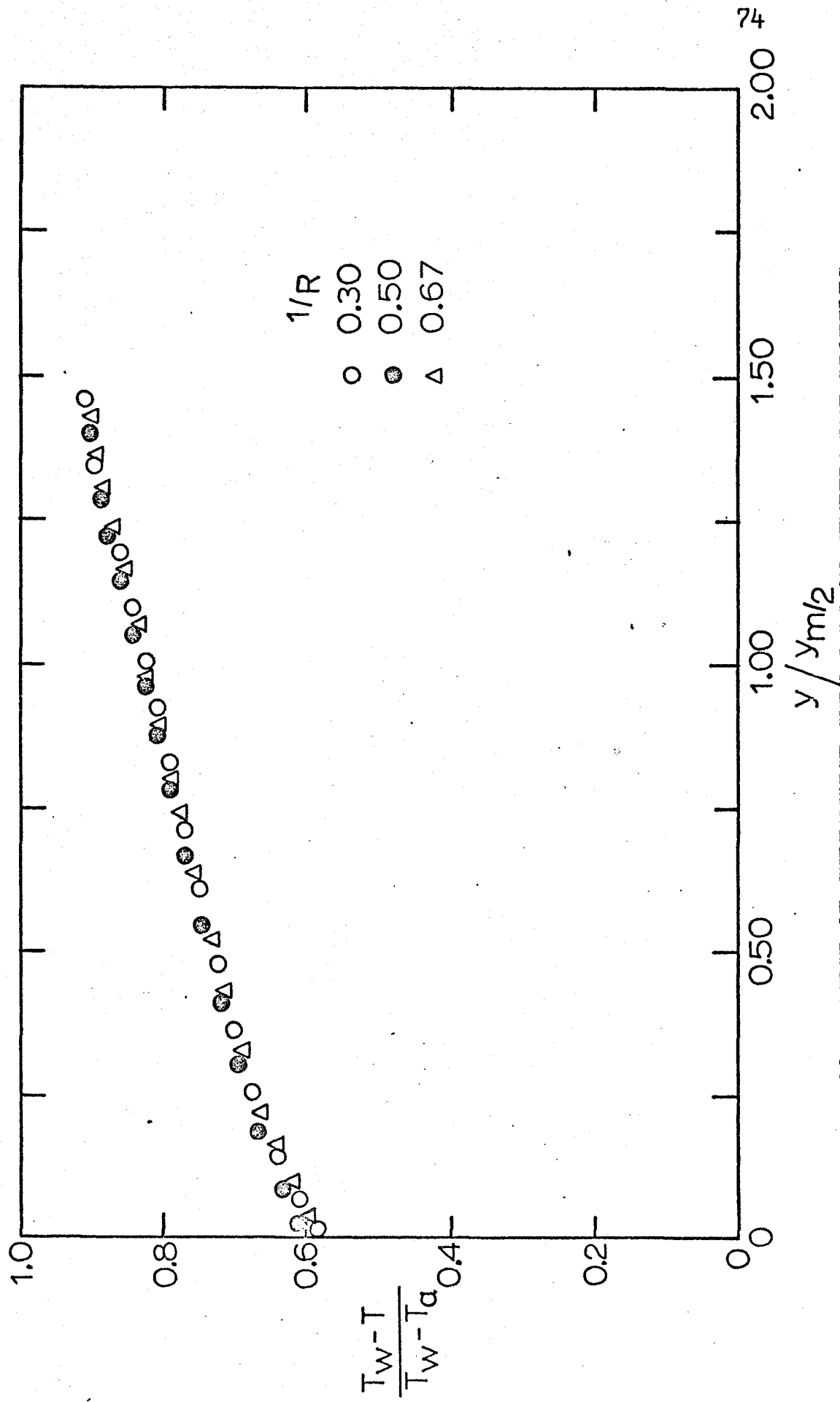


Fig. 22 EFFECT OF STREAMWISE CURVATURE ON TEMPERATURE PROFILES
 0.250 in. nozzle, 60°F HOT RUN, $\theta = 45^\circ$

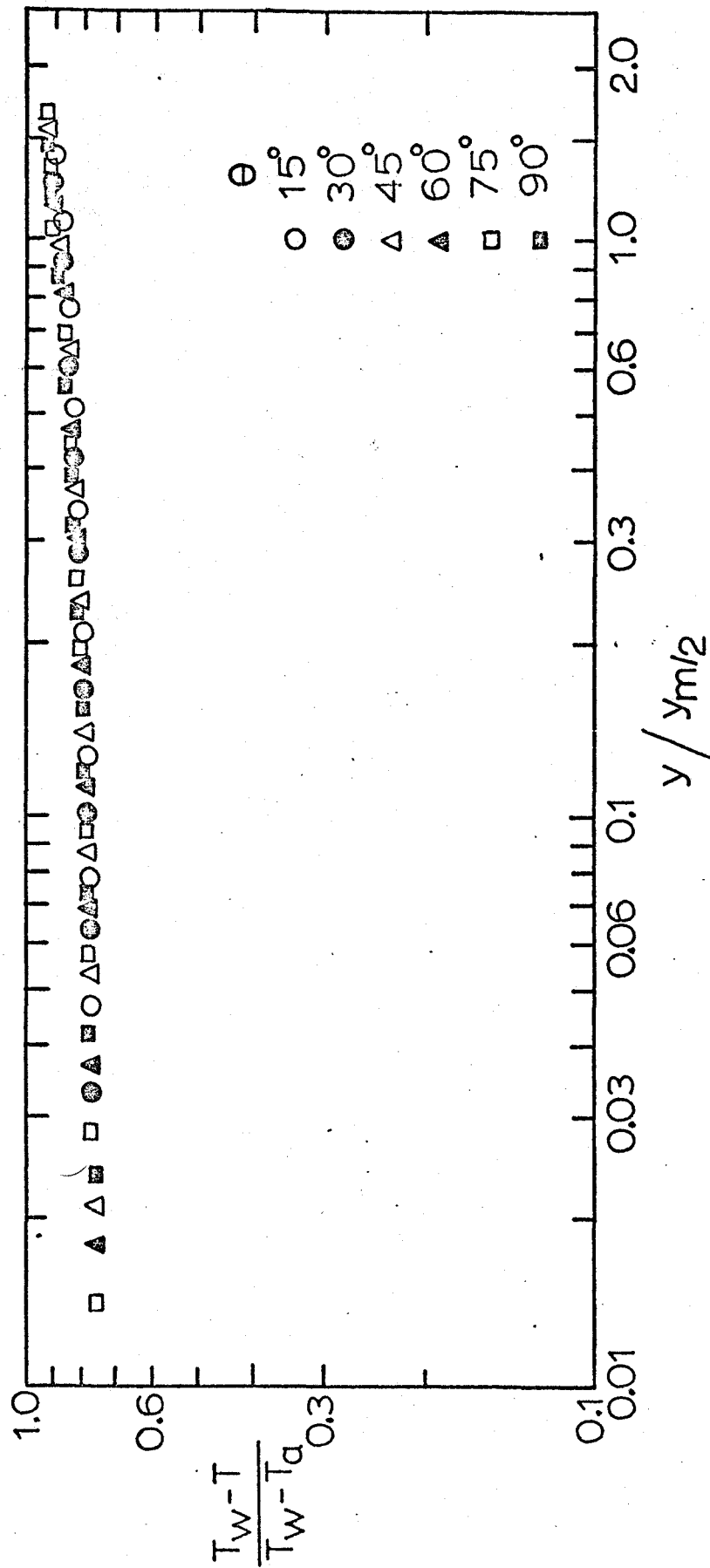


Fig. 23 LOGARITHMIC TEMPERATURE PROFILES
 6.63 in. cyl., 0.089 in. nozzle, 60°F HOT RUN

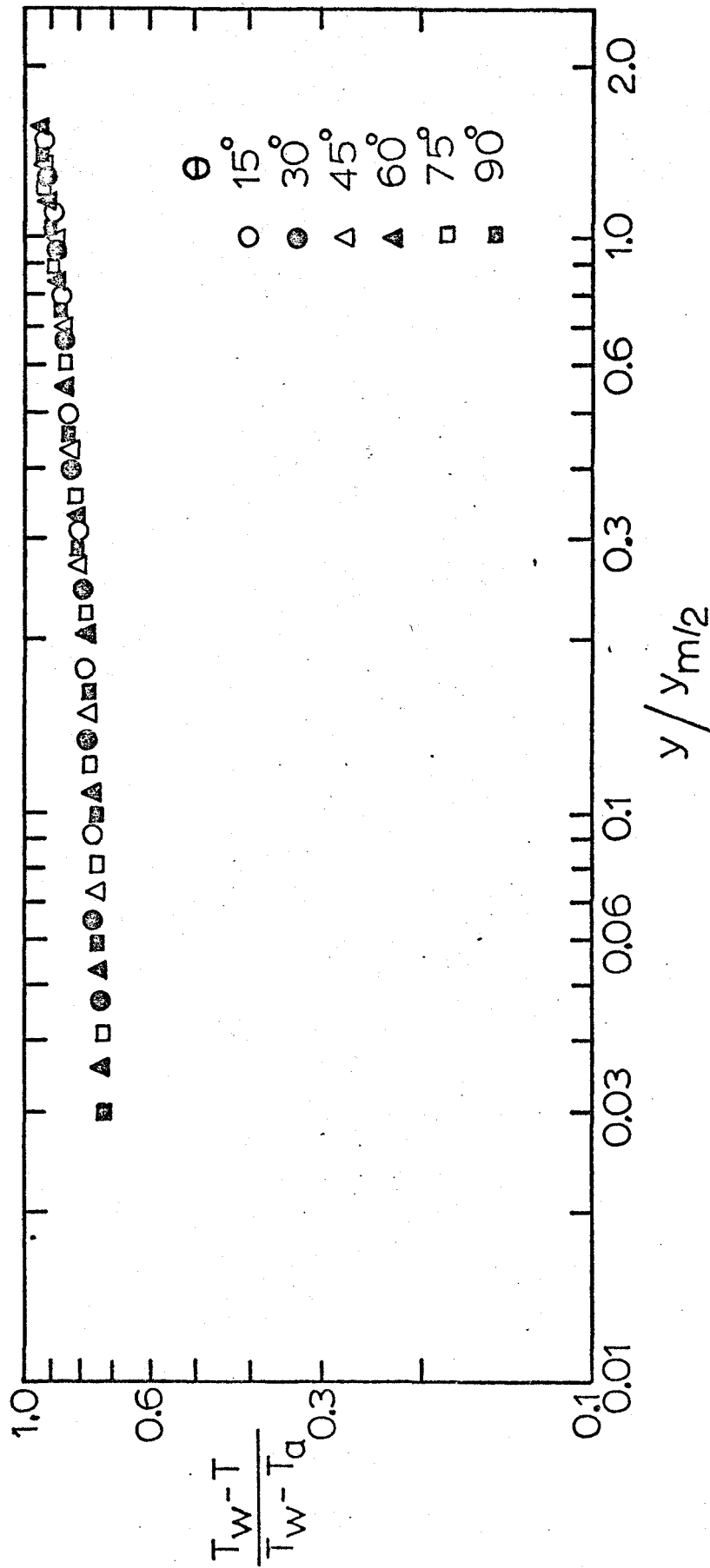


Fig. 24 LOGARITHMIC TEMPERATURE PROFILES
4.00 in. cyl., 0.089 in. nozzle, 60°F HOT RUN

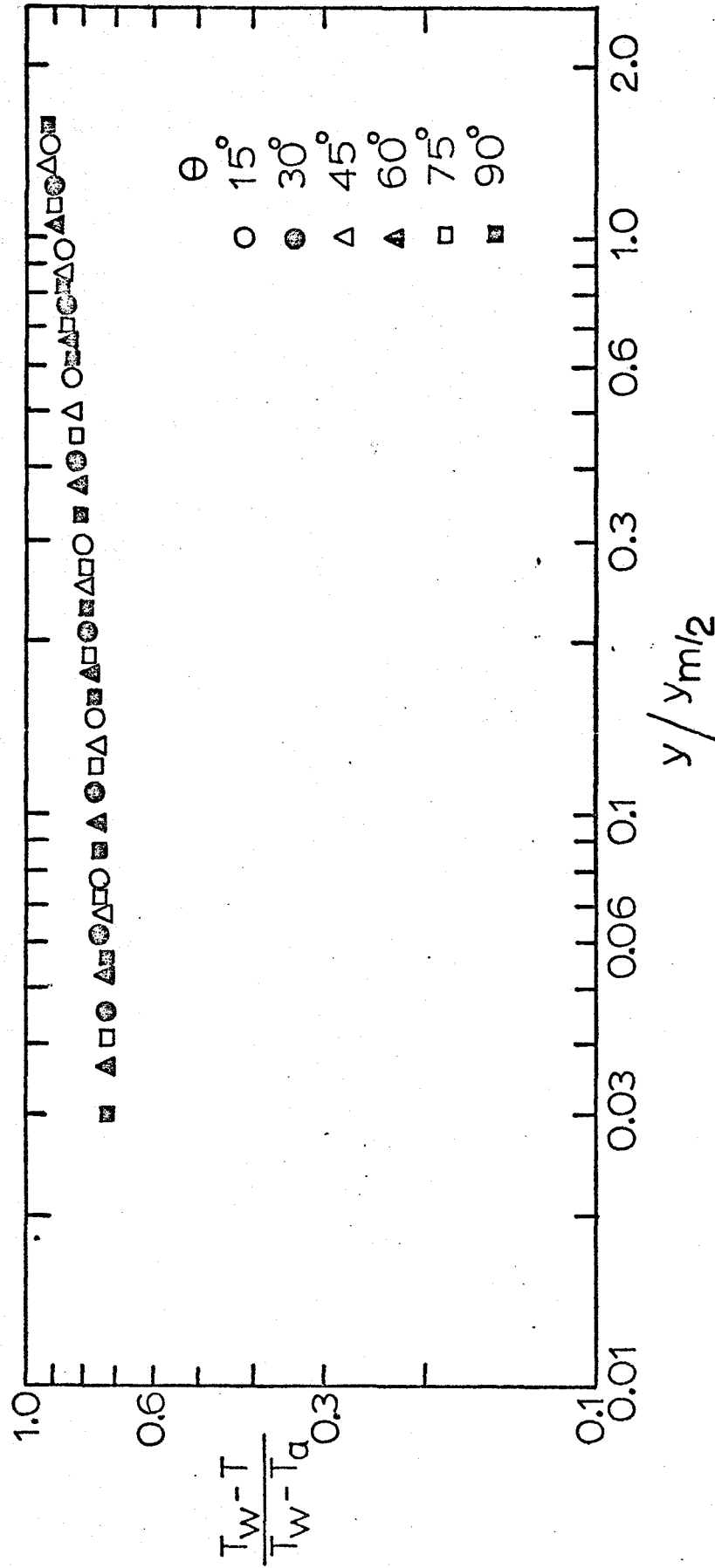


Fig. 25 LOGARITHMIC TEMPERATURE PROFILES
 3.00 in. cyl., 0.089 in. nozzle, 60°F ICI T RUN

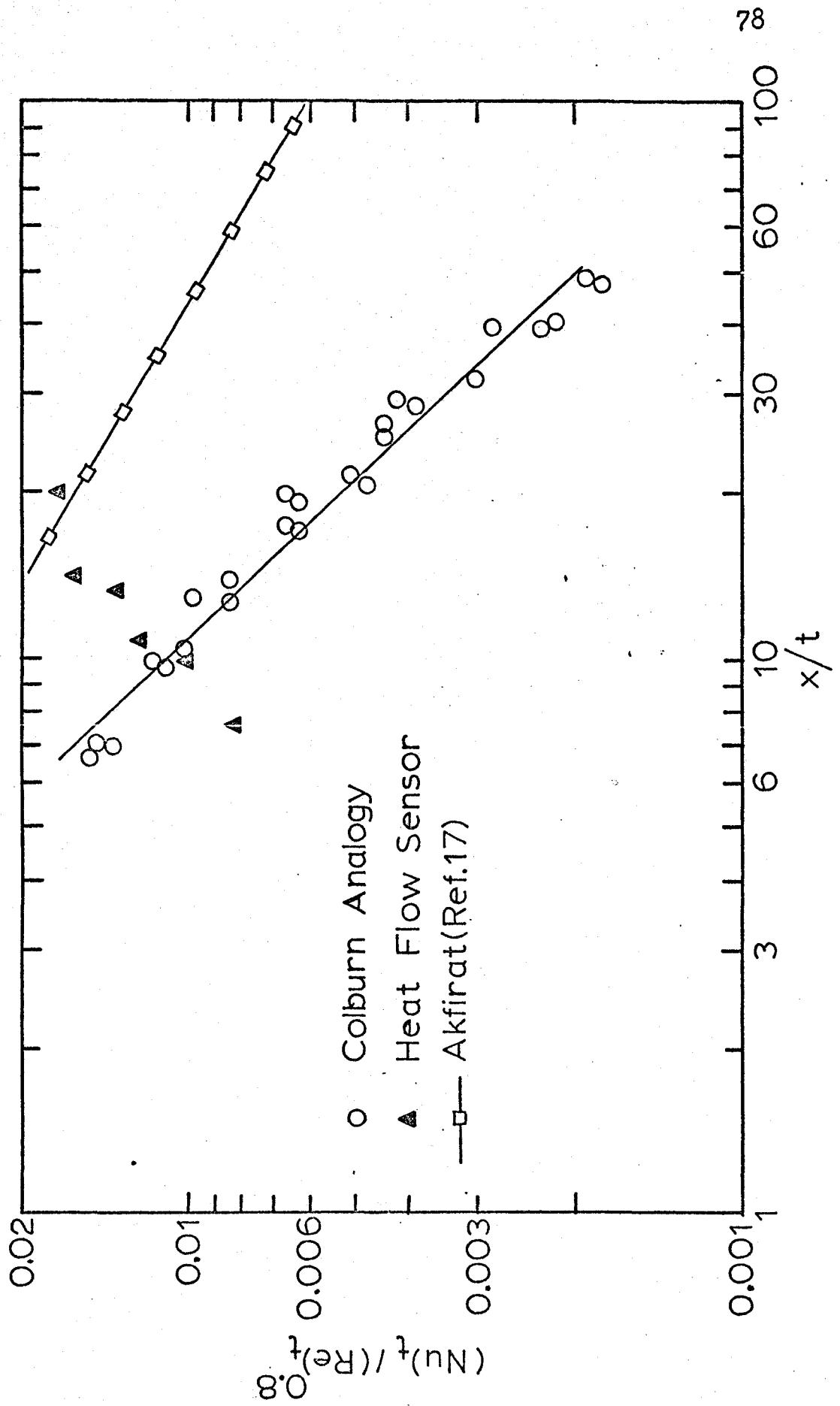


Fig. 26 HEAT TRANSFER CORRELATIONS
(6.63 in. cylinder and Plane Wall Jet)

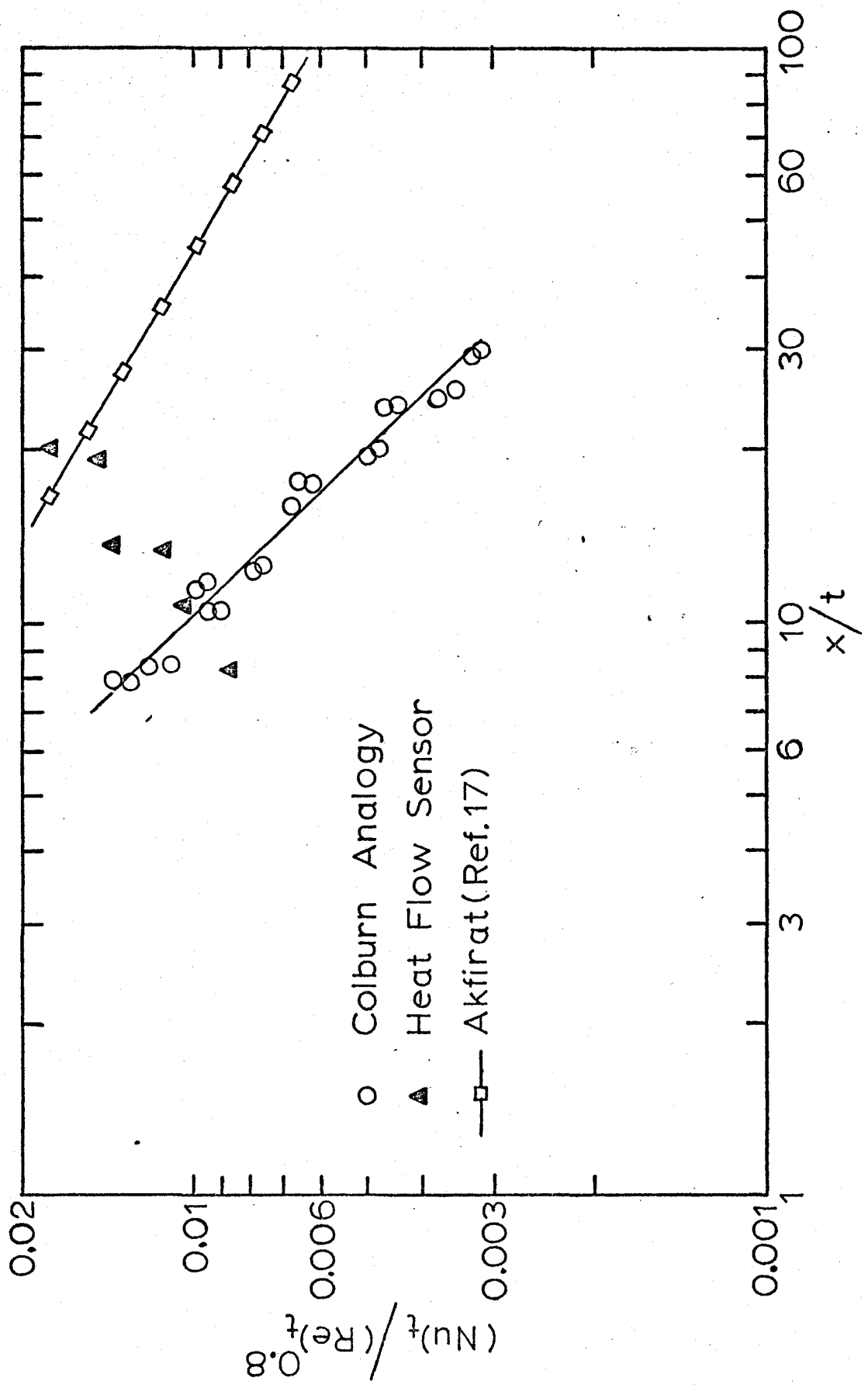


Fig. 27 HEAT TRANSFER CORRELATIONS
(4.00 in. cylinder and Plane Wall Jet)

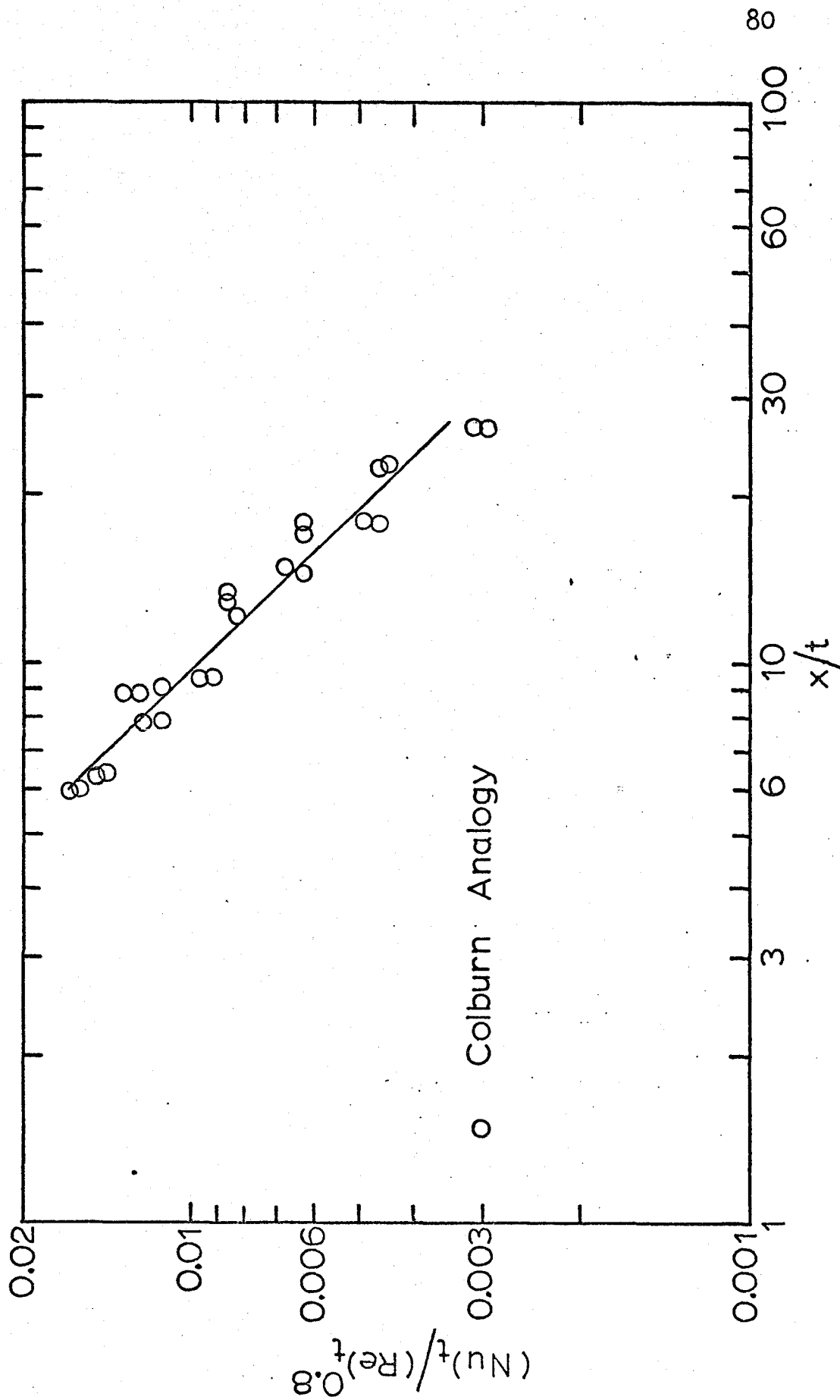


FIG. 28 HEAT TRANSFER CORRELATION
3.00 in. cylinder

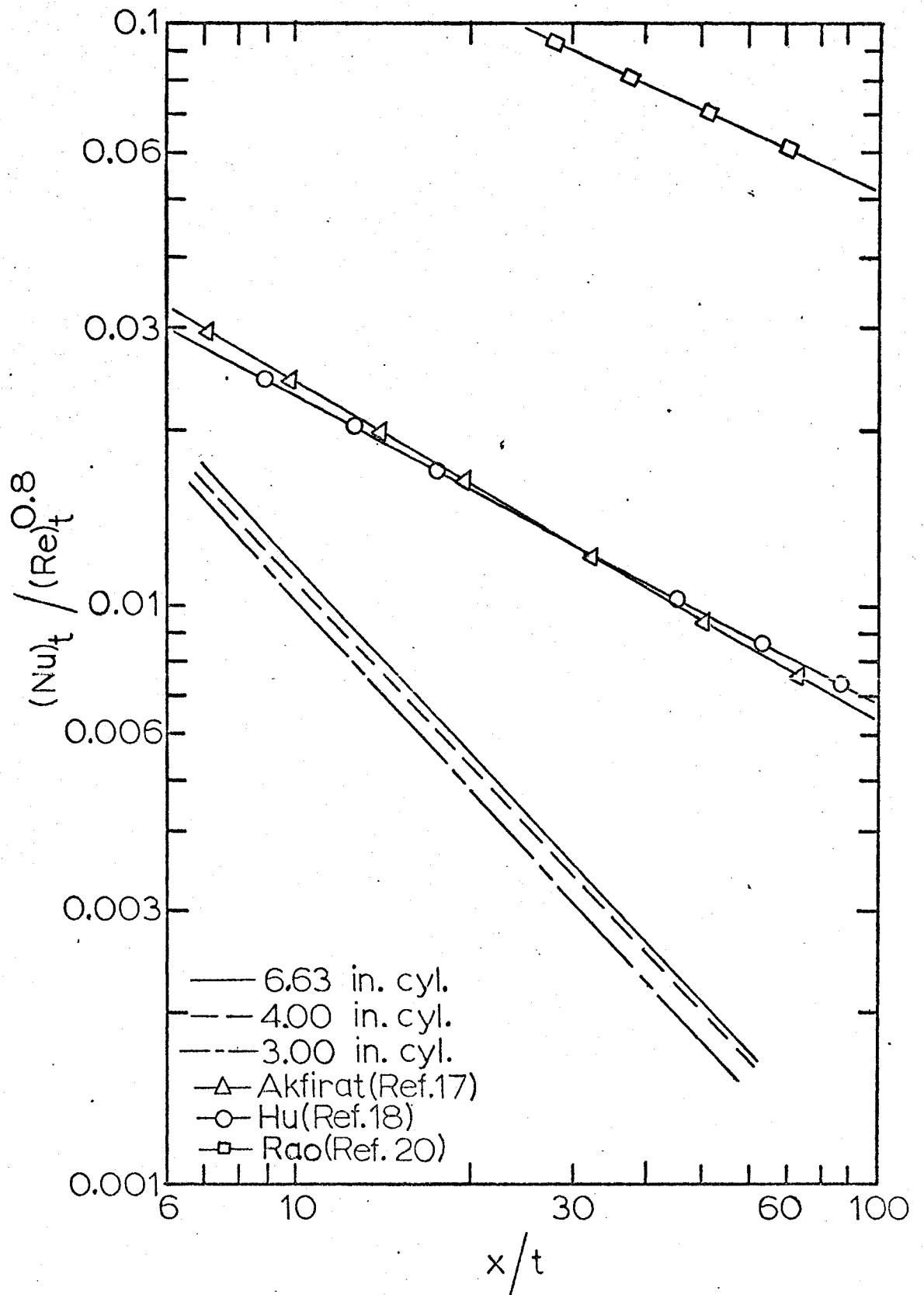


Fig. 29 COMPARISON OF HEAT TRANSFER CORRELATIONS

VITA AUCTORIS

- 1946 Born in Chatham, Ontario on May 25.
- 1964 Completed high school at Chatham Collegiate Institute, Chatham, Ontario in June.
- 1968 Received the degree of Bachelor of Applied Science in Mechanical Engineering from the University of Windsor, Windsor, Ontario.
- 1971 Currently a candidate for the degree of Master of Applied Science in Mechanical Engineering at the University of Windsor.